Bollettino di Geofisica Teorica ed Applicata Vol. 62, n. 1, pp. 33-60; March 2021
DOI 10.4430/bgta0344

Site characterisation in Durrës (Albania) from a seismic microzonation perspective

M. Mancini[1], K. Skrame[2], M. Simionato[1], R. Muçi[2], I. Gaudiosi[1], M. Moscatelli[1] and S. Daja[2]

[1] *Institute of Environmental Geology and Geoengineering, Italian National Research Council, Roma, Italy*

[2] *Department of Applied Geology Environment and Geoinformatics, Polytechnic University of Tirana, Albania*

(Received: 26 April 2020; accepted: 2 October 2020)

ABSTRACT Twenty-nine single-station noise measurements, processed through the Horizontal to Vertical Spectral Ratio (HVSR) technique, a Multichannel Analysis of Surface Waves (MASW) survey, and two 2D array measurements were performed in Durrës to provide useful elements for a geophysical subsoil characterisation. Results from noise measurements defined a zone eastwards of the historical centre, where the characteristics of shallow soil layers are responsible for modification to the seismic response. In particular, HVSR curves in this area showed amplitude higher than 3.4 at a period higher than 1 s. From the analysis of the collected data, four different groups of HVSR curves were recognised, whereas noise measurements were also used to retrieve a preliminary bedrock depth map. These results are potentially useful for correlating construction typologies and vibration period of the buildings with the site amplification and with the damages observed during the seismic sequence for which the highest magnitude event was the M_W 6.2, 26 November 2019 earthquake. Moreover, two shear waves velocity V_S profiles were obtained from a joint inversion of Rayleigh curves with ellipticity. In one case, it revealed the presence of a soil of very poor mechanical properties, which was classified as D soil according to the international codes (EC8, NEHRP); in the other case, the V_S profile allowed us to retrieve important information about the seismic bedrock to be used in numerical modelling for the third level of seismic microzonation.

Key words: ambient vibrations, seismic arrays, site characterisation, Durrës earthquakes.

1. Introduction

Geophysical prospection is widely used after strong earthquakes to evaluate local seismic response and for seismic microzonation (SM) studies (Milana *et al*., 2011, 2020; Gaudiosi *et al*., 2014; Laurenzano *et al*., 2019; Sandron *et al*., 2019; Ashayeri *et al*., 2020; Caielli *et al*., 2020; Giallini *et al*., 2020). Among the most commonly used geophysical methods, the single-station ambient vibrations measurements, analysed with the Horizontal to Vertical Spectral Ratio (HVSR) technique (Nakamura, 1989), are extensively performed in urban areas due to their low cost and high capability to adapt the deployment of the instruments to different logistics,

being non-invasive and easy to perform. Peaks in the HVSR curves may be related to subsurface seismic velocity contrasts, with shallower interfaces producing higher peak frequency f_0. HVSR curves are applicable for many purposes, mostly for evaluating the site resonance frequencies (Mukhopadhyay and Bormann, 2004; SESAME, 2004; Gosar *et al.*, 2010; Caielli *et al.*, 2020) and mapping sediment thickness. Nevertheless, the amplitude of the HVSR curve, depending on the impedance contrast with the bedrock, cannot be used as site amplification. To determine amplification and, in turn, modifications on the ground motion due to the site it is necessary to perform specific local response analyses through numerical modelling of the waves propagation, or in alternative through experimental measures based on earthquake recordings [i.e. Reference Site Spectral Ratio (RSSR) and Generalized Inversion Technique (GIT) analyses]. On this regard, detecting the bedrock depth, by combining ambient vibration measurements with stratigraphic data from boreholes, and reconstructing shear wave velocity (V_S) of the subsoil are essential steps to define geological and geophysical models for simulations.

Within this frame, we present preliminary results obtained from a recent geophysical survey, comprising noise measurements, Multichannel Analysis of Surface Waves (MASW) test, and 2D seismic arrays, carried out on October 2019 in the Durrës municipality, Albania, after the moderate M_L 5.4 earthquake occurred on 21 September 2019. This event, with its aftershocks, commenced a seismic sequence with several relevant shocks until January 2020 and still ongoing with earthquakes with $M > 3.5$. The strongest event of the sequence (M_W 6.2) occurred on 26 November 2019, caused the collapse of many buildings and took 51 lives.

The rationale behind the data acquisition is twofold: i) obtaining useful information for a proper seismic site response evaluation of the study area; ii) investigating the possibility that the observed damages after the September events may be caused, in some cases, by the ground motion amplification due to the shallow subsoil characteristics. In this respect, the results can also be used for individuating or excluding correlations between site effects and the stronger damaging patterns observed during the mainshock of 26 November.

The paper also highlights the fundamental importance of the geophysical investigations in defining the bedrock depth, detecting thickness and lateral variability of the shallow cover deposits, and in providing highlights useful from a SM perspective. In fact, SM defines how local geological and geotechnical characteristics of soils can influence the ground motion at site and modify incoming seismic waves during earthquakes. SM studies, which are at the basis of strategies for earthquake risk mitigation, are structured into three levels, or grades, of increasing complexity and detail (ISSMGE, 1999; Gruppo di Lavoro MS, 2008; Moscatelli *et al.*, 2020): Level 1 and Level 2 allow us to identify zones with similar behaviour on qualitative and semi-quantitative methods, while Level 3 requires a much more accurate approach by means of numerical analyses and modelling in order to evaluate ground amplifications and to obtain response spectra and amplification factors. An in depth geophysical prospection, coupled with an accurate geological subsoil reconstruction, is, thus, useful to provide the basis for a Level 3 SM.

2. Historical seismicity of Durrës and the 2019-2020 seismic sequence

The Durrës municipality is located on a very active seismotectonic belt, where many strong earthquakes occurred in the past, as it is reported in several seismic catalogues (Magnani, 1946;

UNDP, 2003; Aliaj *et al*., 2010). Nine strong earthquakes, with magnitude higher than 6.0, occurred at the city of Durrës from 177 B.C. to 1926. These seismic events had a huge impact on the history and the economic life of Dyrrachium (Durrës) in the antiquity.

Based on the old chronicles, the historians mention the earthquake of 177 B.C. as the very first earthquake to occur in the city. There are only a few passages written by Plutarch about the earthquake of 1 or 2 May 58 A.D., which severely destroyed the city. Afterwards, the earthquakes of 334 and 345 were chronicled. The earthquake of 506 almost completely destroyed the entire ancient city. Considering the importance of Dyrrachium during the ancient period and being it the birthplace of the Byzantine emperor Anastasius I Dicorus, the city was rebuilt completely by the emperor immediately after that seismic event.

The 1 March 1273 earthquake was the hardest one. The city was completely destroyed, hundreds of people lost their lives and the city was abandoned by thousands of people. The earthquakes of 1279, 1869, and 1870 were less destructive and with a lower impact on the life of the inhabitants.

The earthquake of 17 December 1926 with M_S 6.2 and seismic intensity of IX (MSK-64 scale) was the first to be instrumentally recorded, and destroyed many buildings in the cities of Durrës, Kavaja, Shijak, and nearby villages. Many cases of liquefaction phenomena were observed between the city of Durrës and Shijak (Aliaj *et al*., 2010).

The first relevant shock of the 2019-2020 sequence is represented by the M_L 5.4 earthquake, or M_W 5.6 according to Lekkas *et al*. (2019a), of 21 September 2019 with epicentre located close to Durrës downtown (Fig. 1; preferred location and magnitude data from: www.cnt.rm.ingv.it). To this event are correlated a 17-km hypocentral depth and a reverse faulting focal mechanism with a strike slip component. Few minutes later, an aftershock occurred close to the previous epicentre, but with higher hypocentral depth: 29 km. After these first events, the observed permanent environmental effects in the city consisted of weak liquefaction phenomena along the coastal zone, east of the harbour (Lekkas *et al*., 2019a), while damages on buildings were mostly located in the eastern periphery (Fig. 2). The latter are represented by non-structural damages to buildings with reinforced concrete frame, such as detachment of plaster pieces, poundings, and separation cracks between reinforced concrete framing members, and by more severe damages on un-reinforced buildings, i.e. partial or total collapse of load-bearing masonry walls (Lekkas *et al*., 2019a).

The main M_W 6.2 earthquake of 26 November 2019 re-activated the reverse faulting system, as it is shown by the focal mechanism in Fig. 1, and was followed in the next two days by four other events with magnitude higher than 5. The last relevant shock of the sequence is represented by the m_b 5.0 earthquake (www.cnt.rm.ingv.it) of 28 January 2020. The epicentres of the events with magnitude higher than 5.0 are plotted on Fig. 1, and Table 1 shows the parameters of the main events. The variability of location and depth of the hypocentres (Table 1) may tentatively be related either to the progressive rupture of different segments of a single fault or to ruptures of different reverse faults within the local thrust system.

The earthquakes of November induced more severe liquefaction phenomena (i.e. ejection of sand and water from ground fissure cracks, formation of small sand volcanoes and aprons) than the September events and just in the same places (Lekkas *et al*., 2019b; Mavroulis *et al*., 2020). Damages on buildings were extensively located in Durrës, although the very heavy structural damages, i.e. total or partial collapse, were scattered and mostly located east and north of the

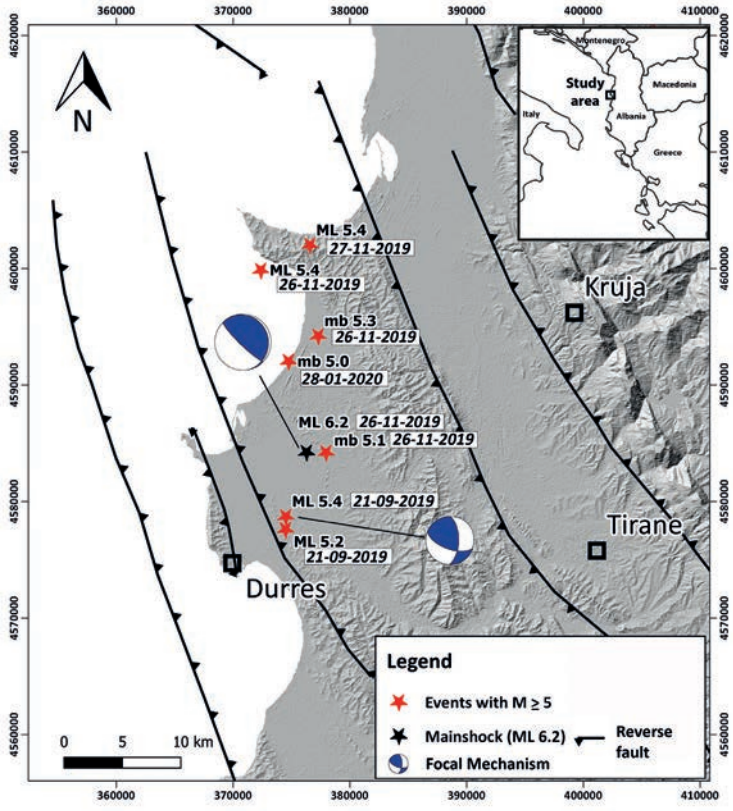

Fig. 1 - Evolution of the 2019 Durrës earthquake sequence (see also Table 1), showing the location of all mainshocks with *M* 5.0 and larger. Focal mechanisms are taken from www.cnt.rm.ingv.it, while active faults in the study area are available from the GEM - GAF (Global Active Faults) project catalogue (partly modified after Weatherill *et al*., 2016).

Fig. 2 - Images of damaged masonry infills of one reinforced concrete building (Rruga Pavaresia) after the 21 September 2019 earthquake.

Table 1 - Summary of the parameters of the largest events of the earthquake sequence (*M* 5.0 and larger). All data are taken from www.cnt.rm.ingv.it. See the text for inferences on location and depth of the hypocentres.

Date	Time (UTC)	Magnitude	Depth (km)	Lat.	Lon.
21/09/2019	14:04:27	M_L 5.4	17	41.35	19.50
21/09/2019	14:15:54	M_L 5.2	29	41.34	19.50
26/11/2019	02:54:11	M_W 6.2	22	41.40	19.52
26/11/2019	02:59:24	m_b 5.1	10	41.40	19.54
26/11/2019	03:03:00	m_b 5.3	10	41.49	19.53
26/11/2019	06:08:22	M_L 5.4	20	41.54	19.47
27/11/2019	14:45:24	M_L 5.4	25	41.56	19.52
28/01/2020	20:15:10	m_b 5.0	13	41.47	19.50

harbour (Lekkas *et al*., 2019b; see also: https://emergency.copernicus.eu/mapping/system/files/components/EMSR412_AOI06_GRA_PRODUCT_r1_RTP01_v1.jpg).

3. Geological setting

The city of Durrës, with its 400,000 inhabitants, is sited along the Adriatic coast of central Albania (Fig. 3a) in a lowland, the Periadriatic depression (Meço and Aliaj, 2000), corresponding to a wide actively subsiding foredeep basin at the outer front of the west-verging Albanides orogenic belt (Ionian and Kruja zones, N-S trending). The chain and the foredeep basin are part of the wider Dinaric-Albanic-Hellenic Arc of the Alpine orogeny, which features a typical thrust-and-fold structural style. Westwards directed compressional movements to the Adria microplate, the inception of which dates back to late Cretaceous, are still active as testified by the strong seismicity. The foredeep basin is filled with more than 2-km-thick marine-to-continental deposits, affected by syn-sedimentary tectonics since the Pliocene. The Pliocene-Quaternary sediments cover with angular unconformity the underlaying Miocene molasse and Jurassic-Paleogene carbonate successions (Fig. 3b).

The city widens partly on a broad alluvial and coastal plain, partly on a western bordering ridge. The plain, late Quaternary in age, is confined by: i) the narrow Mali i Durrësit ridge (187 m high), almost N-S trending from Durrës to Cape Bishti i Pallës, to the west (Fig. 3a); ii) a NNW-SSE directed alignment of low hills from Vrinas to Arapaj, to the east. To the north, the plain is fed by the SE-NW flowing Erzeni River that, along with the Mali i Durrësit promontory and the adjoining beach-ridges facing the Durrës and Lalzit Gulfs, isolates a wide lowland area, the Kënëta e Durrësit, formerly occupied by coastal marshes and ponds reclaimed in the 20th century (Magnani, 1946).

The local relief is strictly controlled by the compressional structures. The western ridge (i.e. the Durresi hills in Fig. 3b) corresponds to the steep, east-dipping and verging, eastern limb of a reverse fault-related anticline, where Messinian-Lower Pliocene successions [Mengaj and Helmesi Formations: Kodra and Naçi (2012)] crop out. The eastern ridge corresponds to the culmination of a gentle anticline at Vrinas; in the middle, a broad syncline is present underneath the coastal-alluvial plain (Fig. 3).

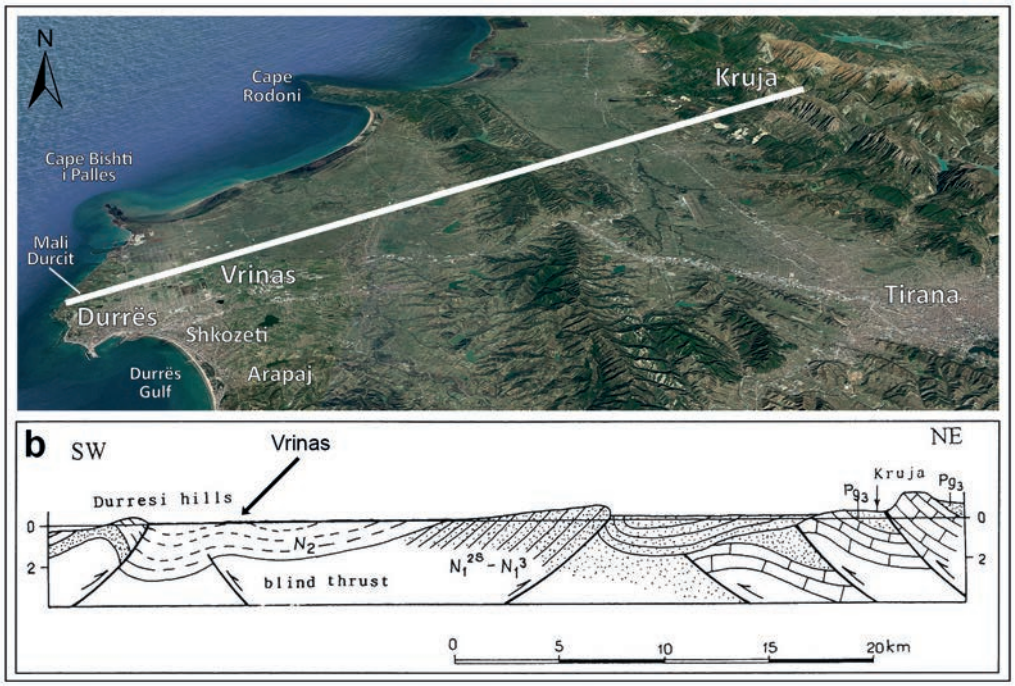

Fig. 3 - a) Tridimensional view from south of the Durrës area, with localities mentioned in the text (image from Google Earth Image©2019TerraMetrics); b) regional scale cross-section showing the structural setting of the Periadriatic basin from Durrës to Kruja [after Aliaj *et al*. (1996) in Meço and Aliaj (2000)]. From SW it is evident the structural setting of the Durrës subsoil, with the NE-verging reverse fault-related anticline (backthrust) of the Durresi hills (i.e. Mali i Durrësit) and the confining large syncline widening up to Vrinas. Pg3: Oligocene siliciclastic turbidites (flysch) covering platform carbonates of the Kruja Nappe (brick pattern); N1: Serravallian-Messinian siliciclastic deposits (molasse); N2: Pliocene-Pleistocene terrigenous foredeep basin deposits.

The Messinian-Pliocene bedrock formations are well exposed on the Mali i Durrësit ridge (Figs. 4 and 5a). At the base it crops out the Messinian Mengaj Formation [unit code N^1_3m(c, d) in Kodra and Naçi (2012) and Naçi *et al*. (2012); Fig. 4], more than 500 m thick, and composed of shallow marine sandstone, conglomerate and clay with gypsum. The overlaying Lower Pliocene Helmesi Formation (up to 1200 m thick) covers with unconformity the Messinian deposits. It is tripartite into: i) a lower transgressive member of shallow marine sand, conglomerate and clay, 50-300 m thick [code N^1_2h(a); Figs. 4 and 5b]; ii) alternated deep marine clay and marl of the intermediate member, 500 m thick [code N^1_2h(b); Figs. 4, 5c, and 5d]; iii) regressive marine sand and clay of the upper member, 400 m thick [code N^1_2h(c)], exposed further east of the study area but present in the subsoil (Fig. 4b). The strongly over-consolidated clays of Helmesi Formation are intensively quarried for brick production (Fig. 5c).

The Quaternary cover overlays with angular unconformity the Messinian-Pliocene bedrock and is represented by loose sediments, mostly marshy-lagoon sand, silt, and clay with peat, up to 130 m thick [unit code $1Qh_2$ in Kodra and Naçi (2012) and Naçi *et al*. (2012); Fig. 4], and by laterally contiguous littoral sands (unit code dQh_2). These littoral sands where affected by liquefaction phenomena after the 2019 earthquakes (Fig. 4), at the backshore of Plazhi i Durrësit and east of the harbour (Lekkas *et al*., 2019a, 2019b). Thin colluvial covers and landslide deposits are present along the hillslopes, where widespread slope instabilities occur.

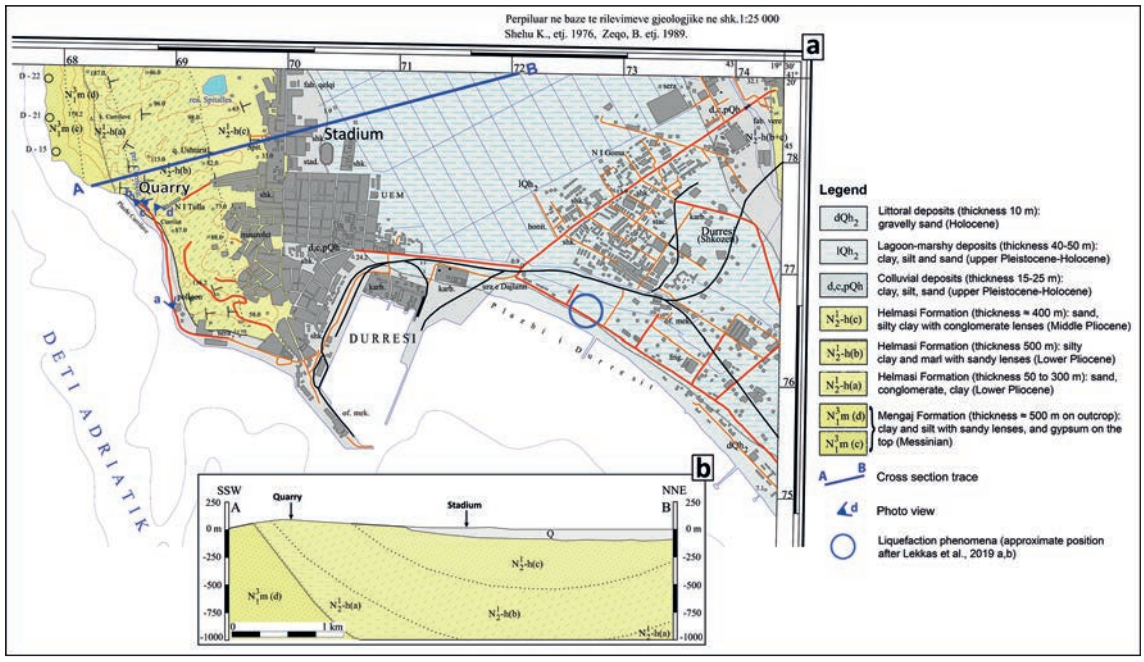

Fig. 4 - a) Sketch of the Geological Map of Albania (scale 1:25,000, Durrës sheet); b) SW-NE trending geological section crossing the city (modified after Kodra and Naçi, 2012).

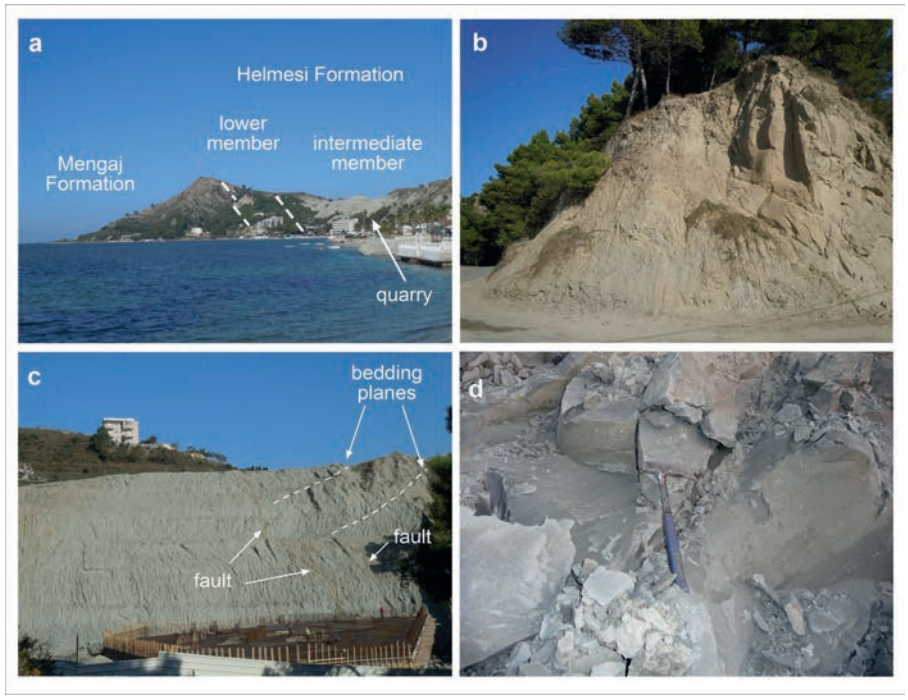

Fig. 5 - Geological bedrock of Durrës: a) view of the Plazhi Currilave beach and the Mali i Durrësit ridge (187 m) from south, with the 40° dipping and eastward tilted Mengai and Helmesi Formations (Messinian and Lower Pliocene respectively); b) lower sandy-clayey member of the Helmesi Formation [code N_2^1h(a) in Kodra and Naçi (2012)]; N5/35 dipping beds; c) view from NW of the NNE-SSW oriented quarry front [Helmasi Formation, intermediate member, code N_2^1h(b) in Kodra and Naçi (2012)]: eastward tilted bedding planes and high angle (reverse?) faults dipping to the west; d) strongly over-consolidated and jointed clays of the Helmasi Formation.

In terms of urban geomorphology, the historical centre of Durrës lays on the eastern lowermost slope of Mali i Durrësit and close to the harbour, whereas in the last decades the periphery has expanded both to the western hilltop (the light-tower neighbourhood), the eastern coastal zone (Plazhi i Durrësit, Shkozeti) and to the inner reclaimed plain areas, to the north. Anthropogenic backfill deposits are widespread all over the urban area and are mostly composed of brick and stone fragments within abundant sand-silt grade matrix. Their thickness is 2-5 m on average, even though locally exceed 10 m in correspondence of archaeological areas (i.e. at the eastern toe of Mali i Durrësit), and close to the harbour.

4. Review of previous available studies

The previous microzonation studies on Durrës date back to Koçiu *et al*. (1985), Koçiu (2004), and Aliaj *et al*. (2010), who mainly focused on the liquefaction potential of Quaternary sediments, depth of the bedrock, predominant period of ground oscillation, and expected seismic intensities (MSK-64 scale).

Three critical areas (Fig. 6a) were recognised (Aliaj *et al*., 2010; Duni and Theodoulidis, 2020): area A, of big deformation on free surface, close to the port, with predominant periods exceeding 0.5-0.6 s, intensities higher than IX MSK-64, and high susceptibility to liquefaction; area B, in the inner plain and easternmost coastal belt, with 0.4-0.5 s predominant period, VIII-IX MSK-64 expected intensity, and moderate to low susceptibility to liquefaction; area C, corresponding to the hills with more than 15° dipping slopes. An equal depth contour map of the top of the

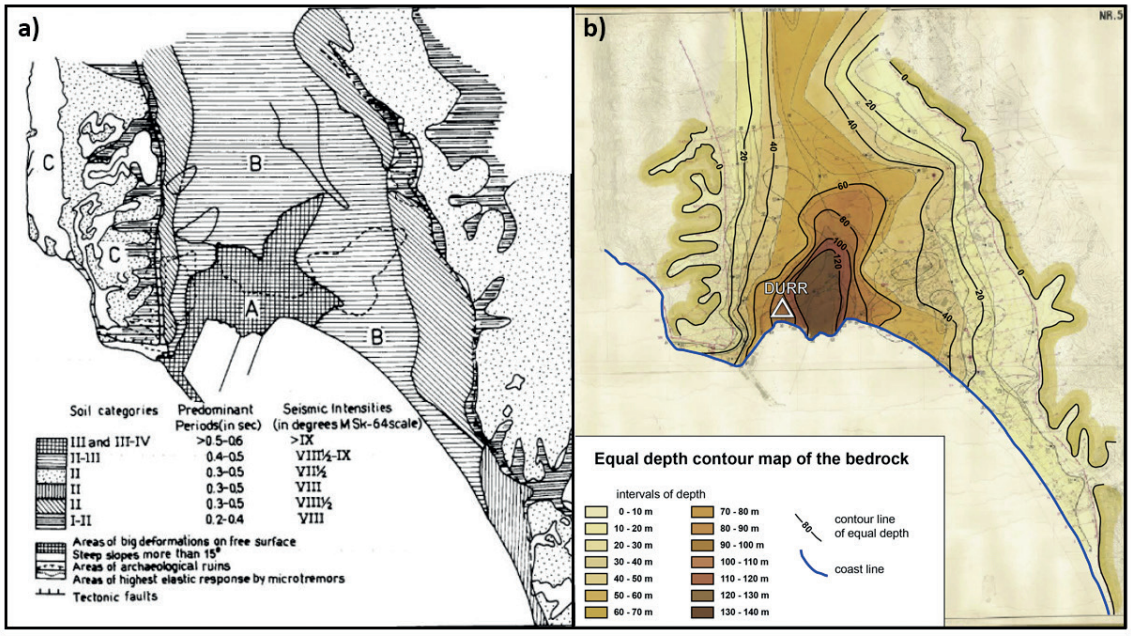

Fig. 6 - First microzonation studies for the city of Durrës [modified after Koçiu (2004) and Aliaj *et al*. (2010)]: a) map of the soil categories and related predominat periods (in s) and seismic intensities; b) equal depth contour map of the bedrock showing the location of DURR seismic station (modified after Duni and Theodoulidis, 2020); depth is referred to the ground.

Pliocene bedrock (Fig. 6b) was also produced by Koçiu *et al*. (1985). It shows an approximately N-S elongated structure, plunging southwards up to the 140 m depth, which can be interpreted as the wide syncline below the plain. At its hinge zone the thick overlaying Quaternary succession was accommodated.

Despite useful tools, for the technicians who are responsible for earthquake-resistant design, may now adequately take into account the local geology influence, thanks to the introduction of seismic response analyses in the international and national prescriptions (BSSC, 2003; CEN, 2004), the results proposed by Koçiu *et al*. (1985) and Aliaj *et al*. (2010) are yet reference studies, especially from a SM perspective.

5. Data set of geophysical measurements

Between 13 and 15 October 2019, a series of twenty-nine ambient vibration measurements was deployed in Durrës. Twenty-four of them (DU01-21 and DU27-29 in Fig. 7) were carried out within an area of approximately 3 km^2, which extends across the whole historical centre. Other five measurements (DU22-26 sites in Fig. 7) were acquired at the eastern periphery, in Rruga Pavaresia at Durrës beach neighbourhood, the most damaged part of the city after the *M* 5.4 event of September.

The equipment consisted of SS02 SARA velocimetric sensors with a cut-off frequency of 0.2 Hz, connected to six-channels SL06 SARA data loggers. Data were recorded with a sample rate of 200 samples per second. During installation, small holes were dug to accommodate the sensors

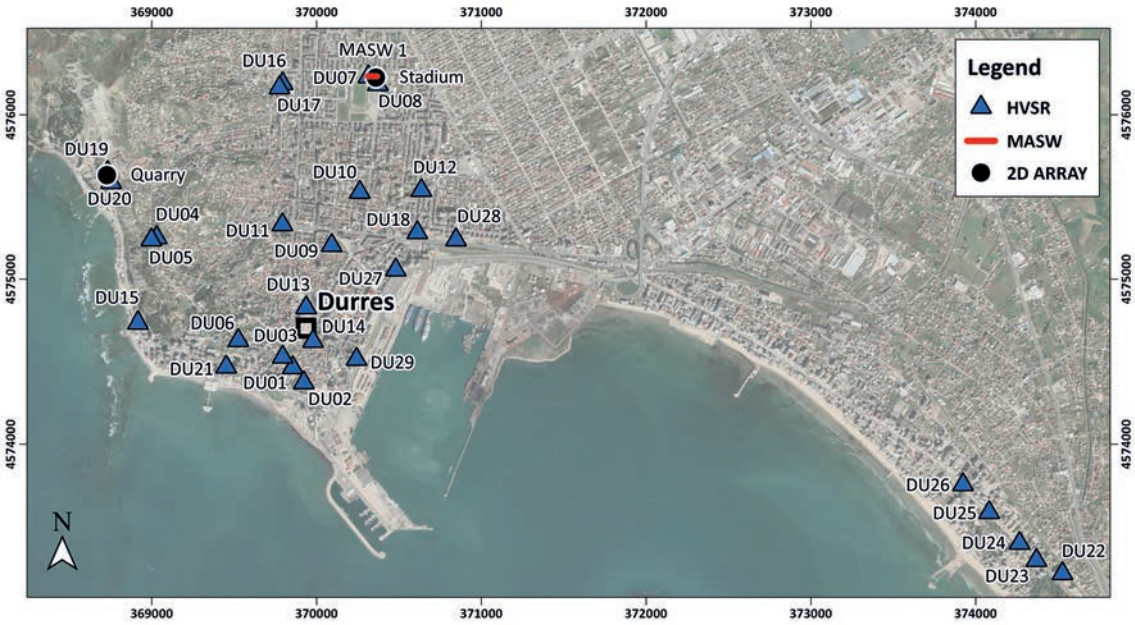

Fig. 7 - Map of the geophysical measurements performed in Durrës. Noise measurements at single station and centres of the small aperture arrays are indicated with blue triangles, and black circles, respectively. MASW active array location is marked with a red line.

on the ground whenever possible, while, being most of the measurements carried out in urban environment, usual care was adopted in deploying the sensors and guaranteeing adequate coupling with the cement, pavement, and asphalt. Care was taken also at ensuring to avoid placement of sensors directly over utilities or disturbances sources.

Recordings of about forty minutes of ambient vibrations were collected and HVSR technique was applied (Nakamura, 1989; Lunedei and Malischewsky, 2015; Sánchez-Sesma, 2017; and references therein). The technique is a well-established approach from which it is possible to retrieve peaks in the HVSR curves that can be related to subsurface seismic velocity contrasts: for instance, shallower interfaces produce higher peak frequencies. Detecting the relations between interfaces and peak frequencies was the main goal of this study.

The choice of investigating the eastern periphery was related to the aim of searching any eventual correlation between the observed damages after the event of September and the presence of peculiar soil resonance periods. This can be done by comparing the soil resonance periods, identified in the HVSR curves to the number of floors of the buildings in the area, which is possible related to building vibrational periods (Gallipoli *et al*., 2020).

Moreover, two V_S profiles were obtained in correspondence of the main stadium of the city and of an accessible clay quarry (Figs. 4, 5c, and 7). They were retrieved from a joint inversion of Rayleigh dispersion curves with ellipticity. Dispersion curves were obtained from 2D array measurements of geophones (Foti *et al*., 2011), in one case (for the stadium site) further joined with a curve from a MASW measurement (Park *et al*., 1999). The geophones were arranged in a two-dimensional geometry, L-shaped with different spacing: 5 m on the long side, 3 m on the other side. The registrations of the noise wave-field were performed for a minimum duration of 40 minutes with 24 geophones (cut-off frequency equal to 4.5 Hz) in both cases. Usual care was adopted in deploying the geophones to guarantee adequate coupling with the ground. Location of the 2D arrays measurements were opportunely chosen to have geologically reliable control points useful for constraining the subsoil model: the stadium array is representative of the Quaternary cover sediments, whereas the quarry array is representative of the geological bedrock.

5.1. Noise measurements

Each ambient vibration recording was divided into 25-s-long time windows through the open-source software Geopsy (http://www.geopsy.org/). We computed amplitude spectra for the vertical and horizontal components (north and east components). Spectra were smoothed using the Konno and Omachi (1998) window with *b* value 40, while the horizontal spectra were computed from the north and east components as $\sqrt{(\text{north}^2 + \text{east}^2)}$ before computing the HVSR for each time window. Then, we computed the average HVSR for each station. Results from noise measurements in terms of HVSR, single spectra, and rotational HVSR are reported on Figs. 8, 9, and 10, respectively.

The obtained HVSR curves showed maximum values between 2.0 and 3.4 in the range 0.4-10.0 Hz. Moreover, some of the HVSR curves are characterised by a large standard deviation, especially at frequencies lower than 1 Hz. Wind blowing could have affected two of the measurements (DU04 and DU05) at frequency lower than 0.4 Hz.

A joint observation of HVSR, single spectra curves, and rotational HVSR has revealed an industrial disturbance at about 1.5 Hz at DU19 and DU20 stations (likely due to working engines

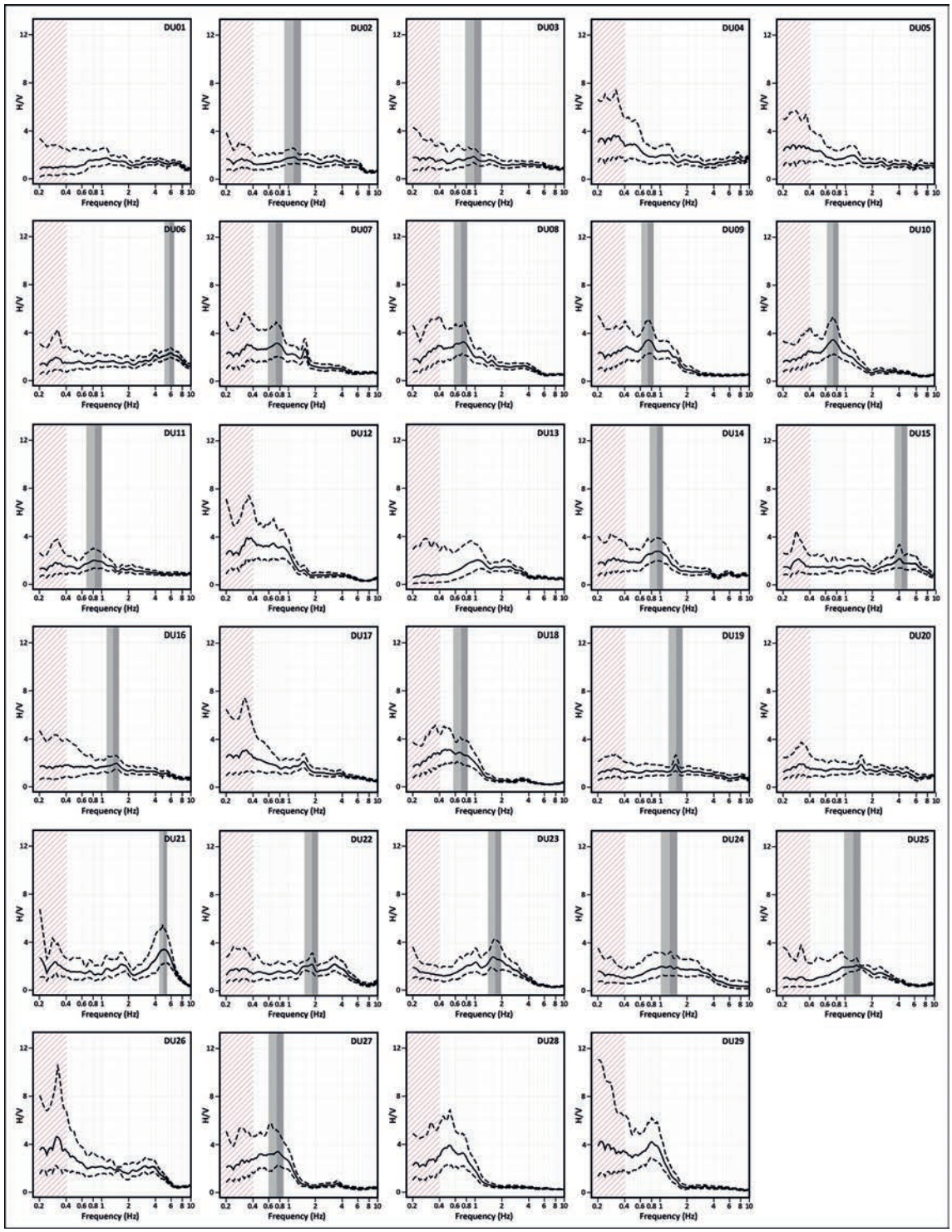

Fig. 8 - HVSR curves computed for the average horizontal components for each station. The vertical grey line shows the evaluated value of f_0.

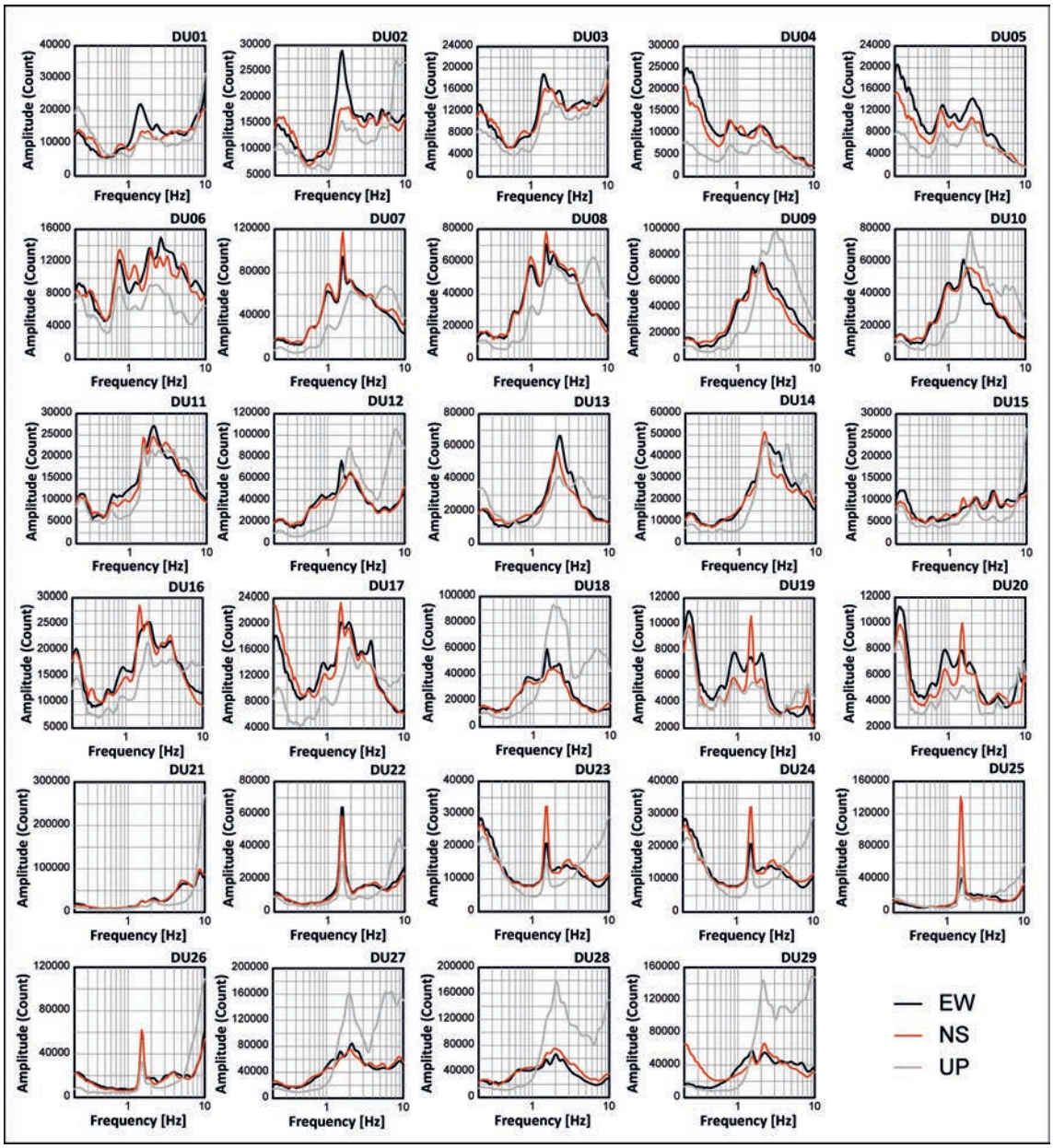

Fig. 9 - Single spectra curves for E-W (black curves), N-S (red curves), and vertical component (grey curves) for each station.

in the quarry), while measurements at DU22, DU23, DU24, DU25, and DU26 presented a clear anthropic peak at the same frequency (1.5 Hz) that we relate to the nearby infrastructures.

The complexity of operating in an urban environment is enhanced by a peculiar feature, visible in the HVSR curves: there are amplitudes lower than 1 at higher frequencies. This is generally linked to the presence of V_S inversion at depth below the measurements, likely expected in highly heterogeneous anthropogenic deposits, or to the presence of pavements and asphalt (Di Giacomo *et al.*, 2005; Castellaro and Mulargia, 2009).

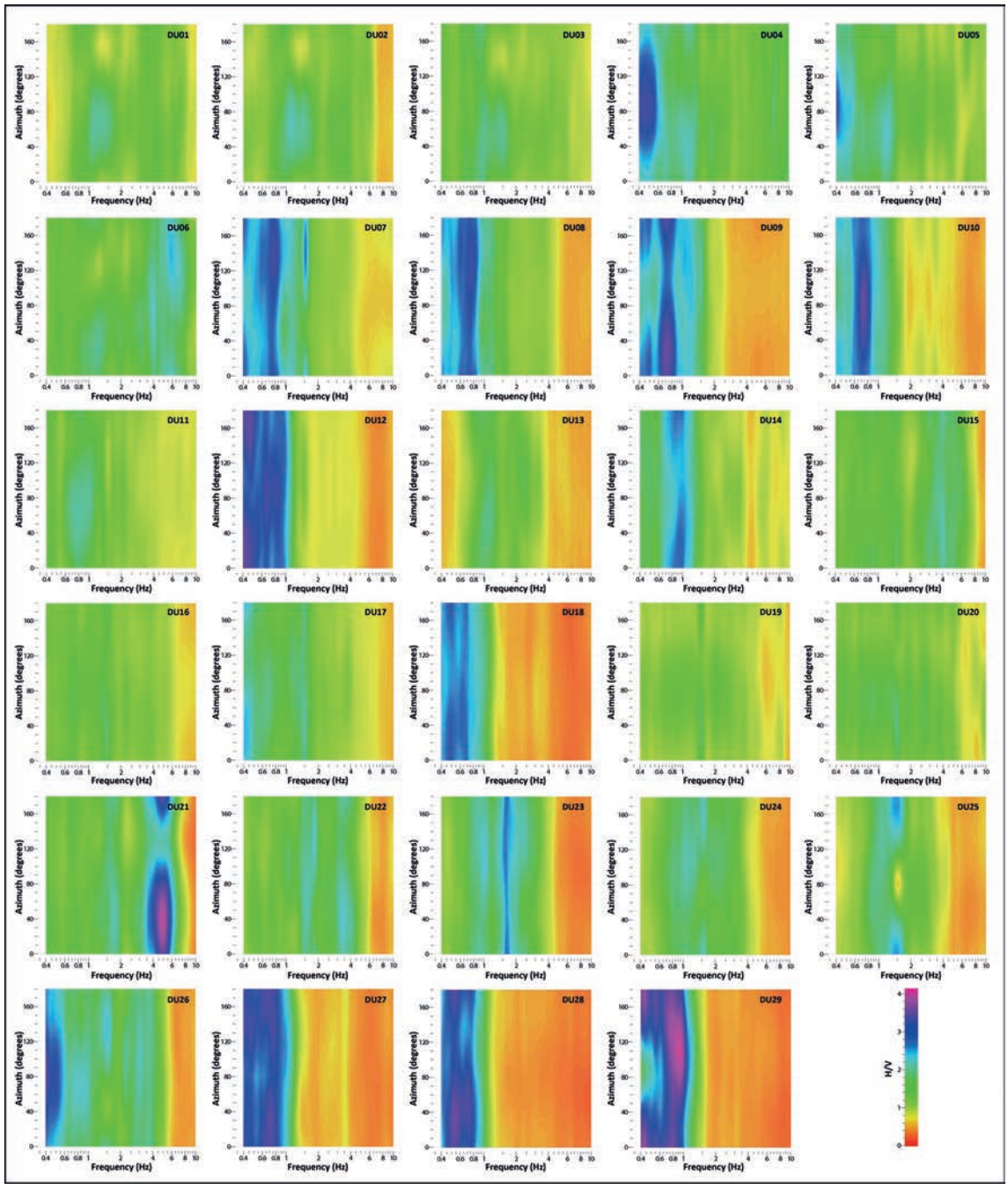

Fig. 10 - Rotational HVSR results for each station: spectral ratios as a function of frequency (*x* axis in Hz) and direction of motion (*y* axis in angle).

Furthermore, the analysis of the horizontal polarisation angles was also performed. The range below 0.4 Hz was excluded from the plot of Fig. 10 in order to correctly enhance graphically any eventual rotational peak. No evident trend is distinguishable, but few measurements (namely, DU06, DU09, DU10, DU11, DU13) in the historical centre showed polarisation angles,

highlighting a 40-80° polarisation, likely related to a 130-170° trending tectonic element such as the buried syncline (see in Figs. 3b and 4b).

The software Geopsy automatically scans the average HVSR curve and identifies the frequency *f* at which the maximum amplitude occurs. In this study, the frequency value f_0 is, then, assigned to the lowest fundamental peak of frequency determined for each HVSR curve.

Before interpretation is attempted, we evaluated the quality of HVSR curves according to the SESAME (2004) criteria in terms of reliability and clarity. According to these criteria, curve reliability (i.e. sufficient number of windows and significant cycles for a given f_0, acceptably low scattering among all windows over a given frequency range around f_0) was verified (see Fig. 11, and the electronic supplements ES1 and ES2). This analysis was necessary in order to deserve particular attention to the identification of eventual peaks induced by low frequency disturbances. Then, also the clarity of HVSR peaks (i.e. fulfillment of amplitude and stability criteria) was checked (Fig. 11 and ES1 and ES2). Only the peak read at the DU10 station HVSR curve completely fulfilled all the criteria for a clear f_0 identification. Most of the HVSR curves, in fact, are characterised by broad band peaks and in some cases (i.e. DU24) show plateau-like shapes, which may be related to the 2D/3D underground geological structures and to the low impedance contrasts.

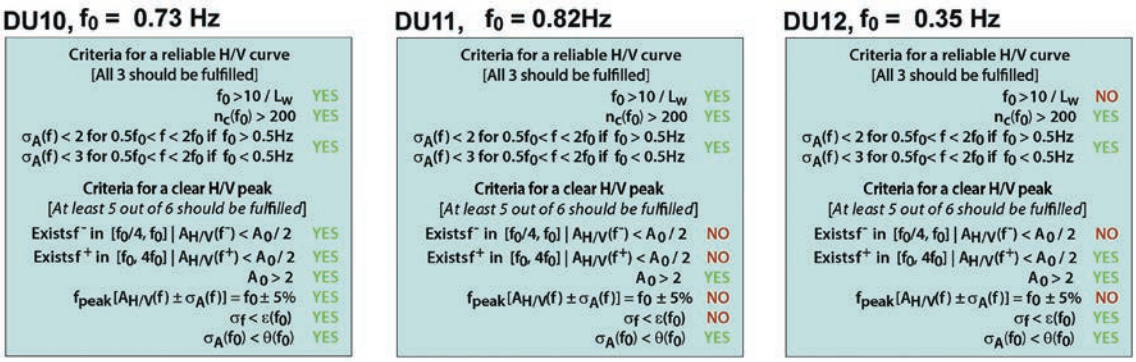

Fig. 11 - Example of graphical representation of the criteria for a reliable and clear HVSR peak recommended by the SESAME research project (SESAME, 2004) for three stations. YES means that the criterium is satisfied and NO shows that the criterium is not satisfied. Results for all the measurements are annexed in the electronic supplements ES1 and ES2.

In order to attempt a possible correlation between subsoil geological surfaces and f_0, a manually adjustment of the peaks was, then, performed, including in the analysis only acquisitions where at least one of the reliability criteria was satisfied. Ten measurements (DU01, DU04, DU05, DU12, DU13, DU17, DU20, DU26, DU28, and DU29) did not satisfy any criteria and, therefore, were excluded by the following analyses. In the graphical representation of the HVSR curves in Fig. 8, the grey vertical band representing the final averaged peak frequency and its standard deviation is reported [only for those ambient vibrations measurements which showed reliable peaks according to the SESAME (2004) criteria]. The average peak frequency is obtained by averaging the peak frequency of all the curves from the individual time windows. Right boundary of the red dashed area represents the threshold value of frequency corresponding to 10/used time windows length (25 s).

On the easternmost and most damaged periphery (DU22 to DU26 sites of Fig. 7), a broader amplitude in the range 1.3-5.0 Hz and characterised by amplitude values lower than 1.0 at frequency higher than 6.0 Hz (Fig. 8) is recognised. The three measurements, DU22, DU23, and DU24, at the eastern periphery showed a reliable peak according to the SESAME (2004) criteria, although noise disturbance sources may have seriously perturbed measurement results, hiding the real amplitude of the peak. A summary of all the frequencies f (where the maximum amplitude occurs) and f_0 (lowest peak with $A_0 > 2$) is reported in Table 2.

Table 2 - Summary of the lowest fundamental peak f and f_0 for each HVSR; f_0 peaks are equal to f except when the amplitude value is lower than 2. In this case, we manually classified the curves as no peak. Only ambient vibration measurement, which showed a reliable peak accordingly to SESAME (2004) criteria were used for the analyses and are reported in the table.

Measure	f	f-stdev	f+stdev	A_{max}	f_0	A_0	A_0/stdev	A_0*stdev
DU02	1.14	0.90	1.38	1.8	no peak	/	1.32	2.55
DU03	0.97	0.77	1.17	1.9	no peak	/	1.40	2.59
DU06	5.70	4.99	6.41	2.4	5.70	2.4	1.99	2.8
DU07	0.72	0.58	0.85	3.2	0.72	3.2	2.02	4.96
DU08	0.70	0.58	0.81	3.2	0.70	3.2	2.23	4.54
DU09	0.73	0.61	0.84	3.4	0.73	3.4	2.31	5.08
DU10	0.73	0.62	0.84	3.4	0.73	3.4	2.25	5.26
DU11	0.83	0.67	1.00	2.0	no peak	/	1.38	2.95
DU14	0.92	0.76	1.07	2.8	0.92	2.8	1.99	3.94
DU15	4.24	3.54	4.93	2.0	no peak	/	1.41	2.88
DU16	1.34	1.13	1.55	1.9	no peak	/	1.38	2.55
DU18	0.70	0.57	0.82	2.8	0.70	2.8	1.99	3.97
DU19	1.50	1.24	1.77	1.9	no peak	/	1.32	2.63
DU21	4.85	4.36	5.35	3.4	4.85	3.4	2.21	5.22
DU22	1.82	1.51	2.14	2.2	1.82	2.2	1.55	3.13
DU23	1.68	1.40	1.96	2.7	1.68	2.7	1.68	4.28
DU24	1.28	1.01	1.55	2.1	1.28	2.1	1.31	3.27
DU25	1.22	0.97	1.48	2.0	no peak (?)	/	1.61	2.56
DU27	0.73	0.59	0.87	3.4	0.73	3.4	2.22	5.21

Afterwards, the corresponding fundamental periods T_0 as $1/f_0$ were computed. This analysis was performed for each noise measurement. In order to map T_0 according to a graphical scale which highlights the main results of the study, in this paper we show on map only the ambient vibration measurements collected in the historical centre and close surroundings (Fig. 12), where all the measures are closely located among each other and almost homogeneously distributed.

We found three trends in the T_0 peaks in the historical centre, that have the significance of areas with homogeneous seismic behaviour for the presence of similar subsoil configurations: i) an area with no significant peaks (yellow circles in Fig. 12); ii) an area with peaks at frequencies in the range 0.1-0.5 s (blue circles in Fig. 12); iii) and the area with peak at very high period (> 1.1 s). Only one measurement showed peak in the range 0.7-1.1 s and it may finally be grouped

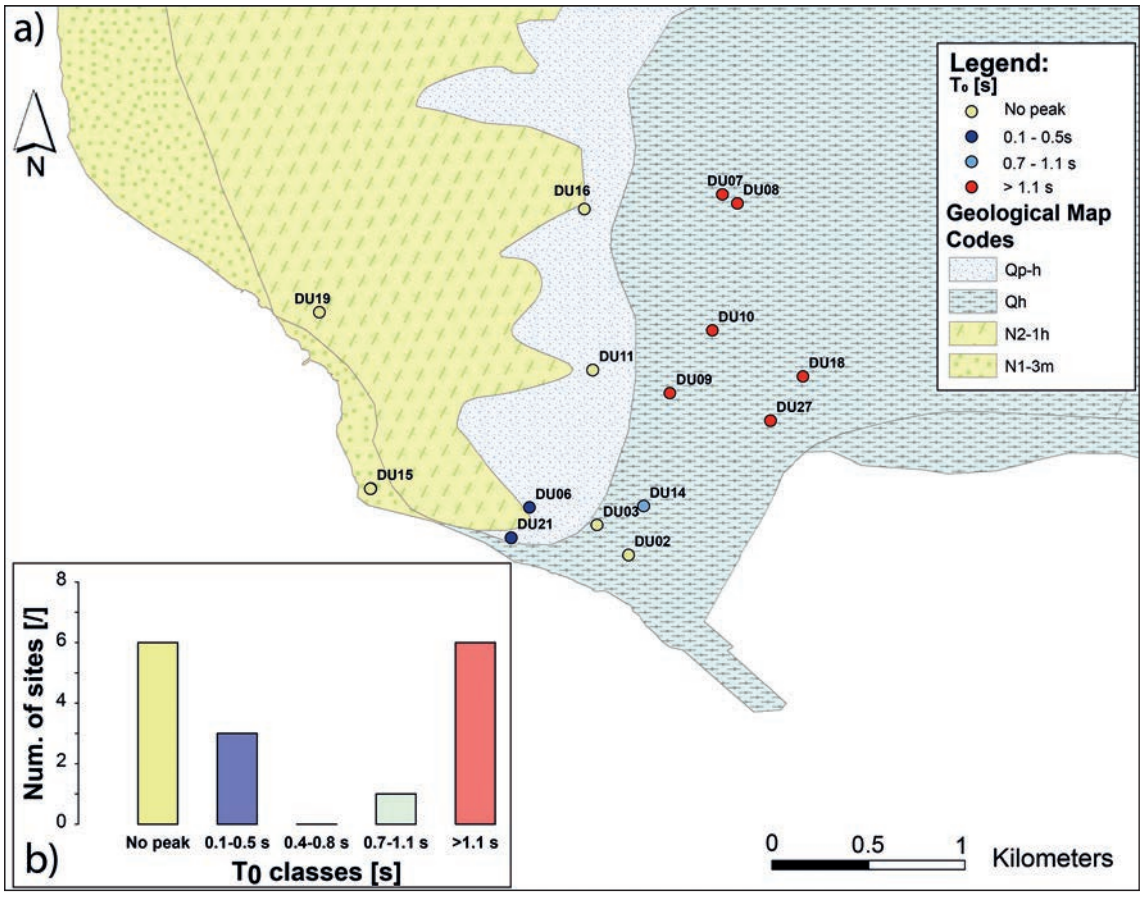

Fig. 12 - a) Fundamental period T_0 map of the sediment layer assessed by HVSR noise measurements (basemap is the simplified geological map of Fig. 5a); b) bar chart of the number of noise measurements. Classes are grouped in: classes of 0.4 s width (0.1-0.5 s; 0.4-0.8 s; 0.7-1.1 s) according to Pergalani *et al*. (2020); no peak class and >1.1 s T_0 class are added respect to this classification (see text for details).

in the > 1.1 s to simplify the result. This behaviour follows the geological map in Fig. 12: on the geological bedrock, i.e. the N1-3m and N2-1h units (Kodra and Naçi, 2012), there is no evidence of peaks in the HVSR curves; conversely, moving towards east, peaks rank to higher periods, indicating a deeper geological bedrock interface below the Quaternary sediments (Qp-h and Qh units of Fig. 12).

Classes of periods T in the range 0.1-1.1 s are grouped according to the suggestion by Pergalani *et al*. (2020): the three intervals (T_1 0.1-0.5 s; T_2 0.4-0.8 s; T_3 0.7-1.1 s) are closely linked to the heights of buildings ($1 \leq T_1 \leq 4$ floors; $3 \leq T_2 \leq 6$ floors and $5 \leq T_3 \leq 8$ floors). Some measurements (DU07, DU08, DU09, DU10, DU11, and DU18) exceeded the 1.1 s limit individuated in Pergalani *et al*. (2020). In fact, classification proposed by Pergalani *et al*. (2020) referred to the most common building heights in central Italy, which has a different level of urbanisation and building typology with respect to Durrës, where more than 8 floors high buildings are not rare. Therefore, we included in the classification a new class with T_0 higher than 1.1 s, and the "no peak" class.

The predominant f_0 frequency in the easternmost peripheral area, out of the map of Fig. 12, ranks between 1.28 and 1.82 Hz, corresponding to a predominant period T_0 between 0.55 and 0.78

s. This evidence, combined with the rough estimate that vibrational periods for buildings of 3-8 floors go from 0.4 to 1.1 s (Pergalani *et al*., 2020), let us hypothesise that resonance phenomena could have taken place in this area, which is characterised by 6-10 floors high and reinforced concrete buildings.

5.2. The array surveys

One of the methods applicable for the purpose of deriving the dispersion curve is the method proposed by Aki (1957, 1965). It is based on the principle according to which the average correlation function between the recordings of isotropic noise, acquired at vertical sensors distributed in different directions at the same *r* distance from a central sensor, has a known form: Bessel function of order 0. The shape of this Bessel function at a given frequency and a given distance *r* is controlled by the phase velocity value. This feature combined with the numerical research of the agreement between experimental data and Bessel function allows us to estimate the phase velocities for each frequency step. When geophones or seismic stations are deployed circularly, the Aki's technique is called SPAC. In fact, in the original formulation, the value of distance *r* in the spatial autocorrelation function is fixed: the stations are all at the same distance from the pole chosen as the origin of the reference system. Ohori *et al*. (2002) and Okada (2003), however, showed that, since the phase velocity $c(\omega)$ is a function of frequency, equivalent results can be obtained by fitting the spatial correlation function at each frequency with the Bessel function that depends on all spatial interdistances [Extended Spatial Auto-Correlation (ESAC) technique]. When different sensor geometry and only specific relative location of the station pairs are taken into account, the technique is called MSPAC (Bettig *et al*., 2005).

Another technique used to identify the dispersion curve is the *f-k* (Lacoss *et al*., 1969). The idea behind this type of processing is to delay the recordings acquired at the different stations of the seismic antenna with respect to a particular wave number vector $\vec{k}$ and to calculate Beam Power (a measure of the signal strength) and Semblance (a measure of coherence) of the outputs thus shifted. By varying many wave number vectors $\vec{k}$, the wave number that maximises the array output (Beam Power and Semblance) can be found in the *kx*, *ky* plane. Simple relationships, then, exist between wave number vector $\vec{k}$ and phase propagation velocity of Rayleigh waves. In this case, however, resolution depends on the interdistances among sensors and on the array aperture that is the largest distance between single sensors.

The basic scheme of the application of all multi-channel seismic antenna techniques consists of the following three steps: i) measuring noise by means of an array of synchronised seismic stations or geophones (seismic antenna) suitably arranged on the surface; ii) estimating the apparent dispersion curve of surface waves; iii) solving the inverse problem to estimate the soil structure looking for the best fit between the experimental and theoretical dispersion curves.

In this paper, aiming at obtaining a robust result, acquisitions by passive 2D array were analysed by *f-k*, ESAC, and MSPAC methods at each site: stadium and quarry. The combination of processing methods (the conventional *f-k* method and the SPAC technique) is highly recommended to increase the confidence about the results (SESAME, 2005).

Different codes were used: 1) Geopsy software (www.geopsy.org) and 2) an ESAC application [developed in the framework of the PRIN-STESSA Project: Mucciarelli (2015)]. The first code was used to retrieve the dispersion curves for: i) applying *f-k* analyses on both active and passive data and MSPAC analyses; ii) solving the inverse problem. The second code was used for the

ESAC analyses. The inverse problem consisted in retrieving the V_S profiles at each investigated sites throughout a joint inversion of Rayleigh dispersion curves with ellipticity.

The results of the analyses obtained at the Durrës stadium (Figs. 4 and 7) from the joint inversion of Rayleigh dispersion curves from MASW and 2D array with ellipticity is shown in Fig. 13. The combination of all the processing methods revealed a satisfactory agreement in this case and all the technique (*f-k*, MSPAC, ESAC) defined comparable dispersion curves. Apparent phase velocity ranks between 100 and about 160 m/s in the frequency range 4.5-10.0 Hz. A power law able to numerically represent V_S value of the best-fit is plotted in Fig. 13e together with the 95% confidence interval of this standard profile. The power law has the form: $V_S = 83\ (1 + z)^{0.355}$, where z is the depth.

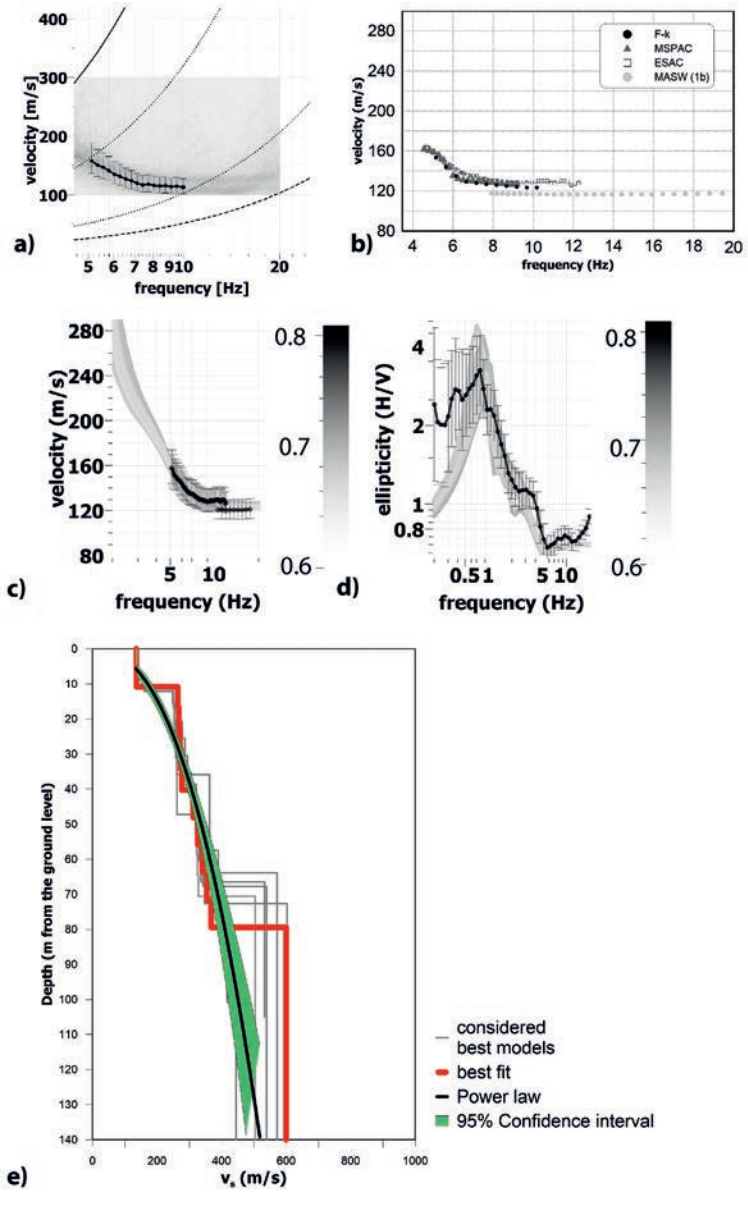

Fig. 13 - Results from 2D array measurement carried out at the Durrës stadium, in the coastal-alluvial plain: a) Rayleigh wave dispersion curve trough *f-k* technique and 2D array limits; b) Rayleigh wave dispersion curves comparison; c) fitting of the dispersion curve; d) fitting of the ellipticity curve; e) considered best V_S profiles (in grey), best fit (in red), power law (in black) in the form: $V_S = 83\ (1 + z)^{0.355}$ and 95% confidence interval of this standard V_S profile.

The V_{S30} (the average shear-wave velocity in the uppermost 30 m) obtained for this site (Table 3) is 180 m/s, corresponding to the soil class D, according to Eurocode 8 [EC8: CEN (2004)]. This confirms the very poor mechanical quality of the marshy soil of the Durrës plain.

The results of the analyses obtained at the quarry site (Figs. 4, 5c, and 7), from the joint inversion of Rayleigh dispersion curves from 2D array with ellipticity at the DU20 site, are plotted in Fig.14. Apparent phase velocities do not significantly vary from 600 m/s in the range 12-15 Hz, while a mismatch between f-*k*/MSPAC and ESAC curves can be recognised in this case. This is a commonly observed feature in experimental results. Out of the resolving power limits plotted in Fig. 14a, the *f-k* dispersion curve tends to 800 m/s, showing similar shapes obtained by the ESAC technique application. The lower bound depicted by the *f-k* technique was chosen to perform the following Rayleigh surface wave inversion. This choice, leading to underestimates of V_S, is supported by the consideration that slightly linear increase V_S with depth are expected, being the subsoil of the site characterised by the over-consolidated and jointed clays of the Helmesi Formation. Local geological indications helped in identifying the most reliable V_S profile in this case. It is worth noting also that ellipticity played only the role of constraining the results for a wider interval with respect to the one due to the used instrument band width (4.5 Hz), since the HVSR curve at the DU20 site is flat. Nevertheless, for a conservative approach, the resulting V_S profile was considered up to 30 m, which is a value overcoming only for few metres the depth defined by the rule of thumb of estimating the maximum depth by dispersion curve (maximum exploration depth $\approx v_{max}/f_{min}/2$).

Table 3 - Stadium site: geological model and V_S profile.

From (m from ground surface)	To (m from ground surface)	Thickness (m)	V_s (m/s)	Geological unit
0.0	2.2	2.2	135	Colluvial and lagoon-marshy deposits (units $1Qh_2$ and d,c,pQh, in Kodra and Naçi, 2012)
2.2	4.4	2.2	135	
4.3	6.5	2.2	136	
6.5	8.7	2.2	136	
8.7	10.9	2.2	136	
10.9	16.9	6.0	136	
16.7	22.7	6.0	264	
22.6	28.6	6.0	267	
28.5	34.5	6.0	270	
34.4	40.4	6.0	273	
40.3	48.3	8.0	276	
48.1	56.1	8.0	312	
56.0	64.0	8.0	326	
63.8	71.8	8.0	340	
71.6	79.6	8.0	354	
79.5	118.5	39.0	368	Silty clay and sand with conglomerate lenses (unit $N^1_2h(c)$, in Kodra and Naçi, 2012)
118.6	157.6	39.0	599	
140.0	179.0	39.0	620	

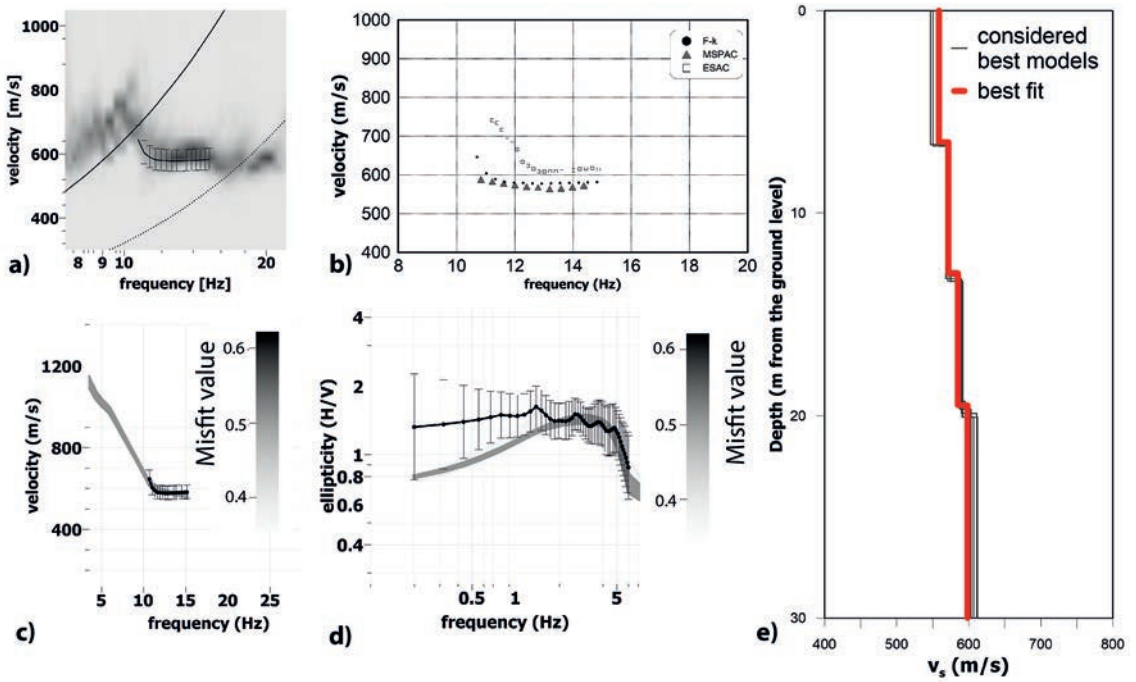

Fig. 14 - Results from 2D array measurement carried out for the Durrës clay quarry, in the Mali i Durrësit ridge (Fig. 5): a) Rayleigh wave dispersion curve trough *f-k* technique and 2D array limits; b) Rayleigh wave dispersion curves comparison; c) fitting of the dispersion curve; d) fitting of the ellipticity curves; e) considered best V_S profiles and best fit.

According to the V_S in Table 4, the V_{S30} is equal to 573 m/s. The individuated EC8 soil class is B, corresponding to the weathered geological bedrock cropping out in the western part of the historical centre along the Mali i Durrësit ridge. This latter V_S profile (Fig. 14d) may be considered as representative of the V_S of the geological bedrock.

Table 4 - Quarry site: geological model and V_S profile.

From (m from ground surface)	To (m from ground surface)	Thickness (m)	V_s (m/s)	Geological unit
0.0	6.5	6.5	559	Clay and marl with sandy lenses (unit N^1_2h(b), in Kodra and Naçi, 2012)
6.5	13.0	6.5	559	
13.0	19.5	6.5	572	
19.5	26.0	6.5	585	
26.0	30.0	4.0	598	

No universal definition, in fact, exists regarding the distinction between geological and seismic bedrock, with the latter having $V_S \geq 800$ m/s. Despite this, it can be assumed that the geological bedrock is the over-consolidated and jointed clays of the Helmesi Formation [N^1_2h(b) and N^1_2h(c) in Fig. 4]. Notwithstanding the V_S are lower than 800 m/s, this site did not show peaks in the HVSR curves (see DU20 on Fig. 8) and the amplifications in Durrës are all expected to be related to the upper Quaternary sediments, absent in the quarry site but present further east in the coastal-alluvial plain.

6. Mapping the geological bedrock depth

The variability of the fundamental resonance frequency over large areas is linked to the subsoil structure (i.e. lateral velocity variations, bedrock morphology of the basin). Therefore, information about the bedrock depth (hereafter *h*) is commonly obtained through a simplified approach (Thabet, 2019; Hinzen *et al*., 2004). It can be demonstrated that a physically plausible f_0 - *h* relationship exists in the assumption of a V_S profile for the sedimentary cover (D'Amico *et al*., 2008) and can be expressed in the form of:

$$h \approx A * f_0^B (1). \tag{1}$$

The same approach was also used in this study. Therefore, coefficients *A* and *B* were chosen by plotting on the plane f_0 - *h* the only available experimental *h* value obtained from the V_S profile for the site that was not deployed on the seismic bedrock (e.g. the stadium noise array), and the corresponding f_0 was derived from HVSR noise measurement. These estimates were, then, compared with the existing linear regressions of literature (Ibs-von Seht and Wohlenberg, 1999; Delgado *et al*., 2000a, 2000b; Parolai *et al*., 2002; Hinzen *et al*., 2004; Birgören *et al*., 2009; Ozalaybey *et al*., 2011; Del Monaco *et al*., 2013; Fairchild *et al*., 2013; Harutoonian *et al*., 2013; Tün *et al*., 2016; Thabet, 2019).

As indicated in Fig. 15a, this representative point is very close to the Delgado *et al*. (2000b) relationship. To confirm the validity of using this relationship in the study area, the power law of the best-fit model of Fig. 13e was used to describe the depth *z* - V_S relationship (Fig. 15b):

$$V_S(z) = V_{S0}(1 + z)^x . \tag{2}$$

Knowing the parameters V_{S0} and *x* in Eq. 2, it is possible to independently obtain the *A* and *B* coefficients in Eq. 1 (D'Amico *et al*., 2008) through the equation:

$$A = \left[\frac{V_{S0} \bullet (1 - x)}{4} \right]^{\frac{1}{(1-x)}} ; \; B = - \frac{1}{1-x} . \tag{3}$$

In this case, V_{S0} being equal to 83 m/s and *x* equal to 0.355, the coefficient *A* results in a value of 56, while the *B* coefficient results in a value of 1.55 (Table 5).

The aforementioned values were compared to the existing correlation coefficients parameters of *f* - *h* relationships of Delgado *et al*. (2000b) defined in Fig. 15a. Coefficients derived from the procedure described above and the existing ones are in good agreement. *A* and *B* coefficients proposed by Delgado *et al*. (2000b) were used to estimate the thickness *h* of the resonant

Table 5 - Derived and existing correlation coefficients parameters of frequency-depth relationships (Thabet, 2019).

Reference	A	B
This study (Durrës stadium V_S)	56	1.55
Delgado e*t al.* (2000b)	56	1.30

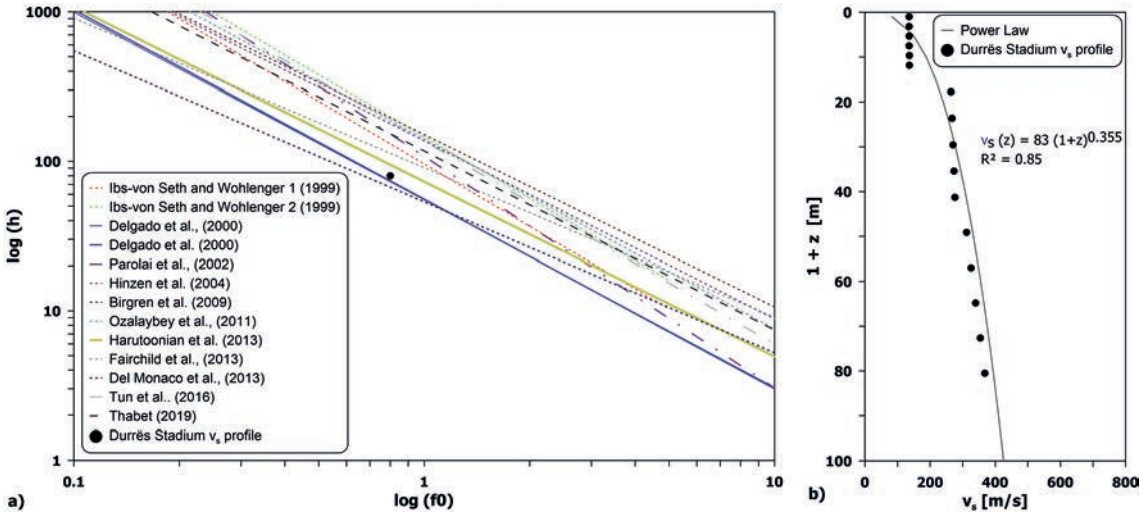

Fig. 15 - a) HVSR resonance frequencies (f_0) versus the bedrock depth (h) from the stadium V_S profile compared with the literature relationship reviewed in Thabet (2019) and reference therein; b) V_S velocity profile at the stadium (black points) and interpolation plot (solid black line).

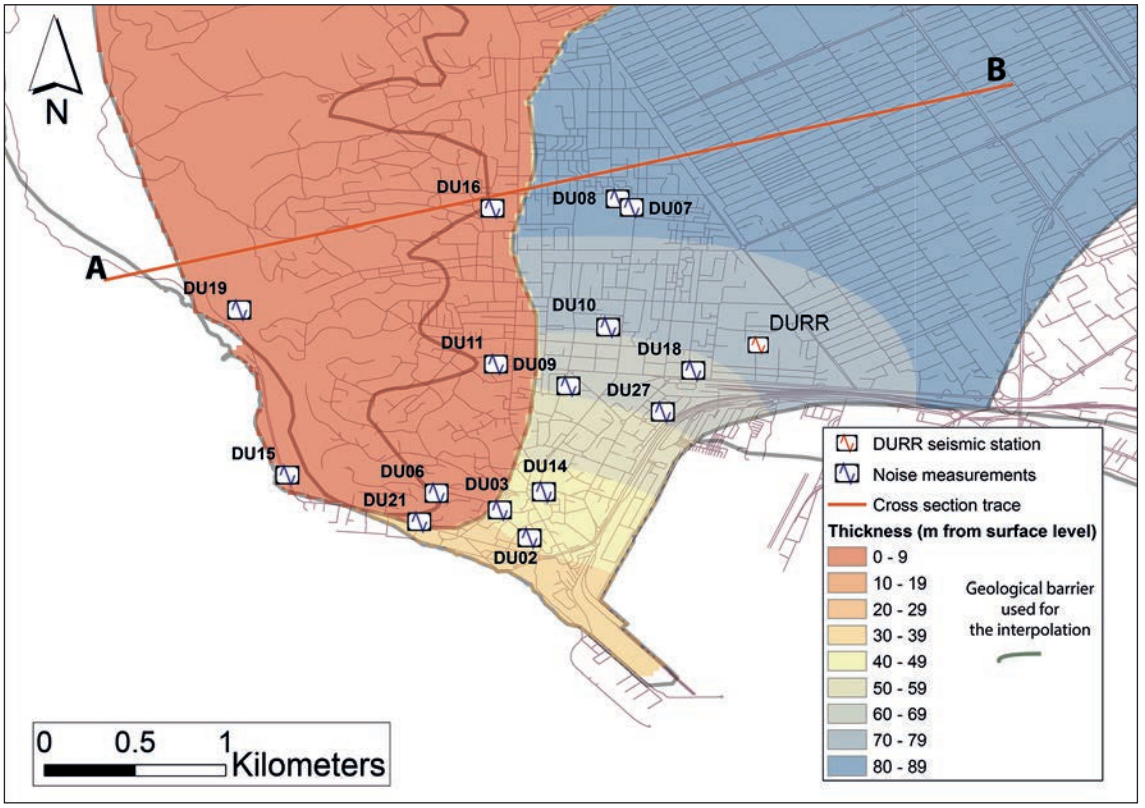

Fig. 16 - Contour map showing the thickness of the resonant cover soil above the bedrock. A geostatistics polynomial algorithm (Diffusion Interpolation) was used to produce the map.

sedimentary layer from HVSR noise measurements over the study area, being they retrieved over a more consistent data set.

Thicknesses *h* obtained through Eq. 1 for each measurement point was used to produce a contour map of the resonant cover soil above the bedrock (Fig. 16). A Local Polynomial Interpolation (Diffusion Interpolation) in the software ArcMap was used to account for spatial distribution and to realise the map. In the absence of barriers, it applies a polynomial interpolation technique that uses randomly distributed measured data to predict (interpolate/extrapolate) values at any un-sampled location within the area of interest. Not to cross different geological formations and to bound the interpolation inside a homogeneous area from the geological point of view, we used geological limits as boundaries for the prediction. Local polynomial algorithm makes use of the spatial dependencies of the measured values in these cases.

The results of the interpolation are plotted on the map in Fig. 16 in terms of cover soil thickness. A somewhat similar trend to the one noted by Koçiu *et al*. (1985) and Koçiu (2004) (Fig. 6b) can be recognised: maximum thickness of the resonant cover, and maximum depth of the bedrock, is located at the north and east of the harbour-railway station zone (DU18 and DU27) and of the DURR permanent seismic station.

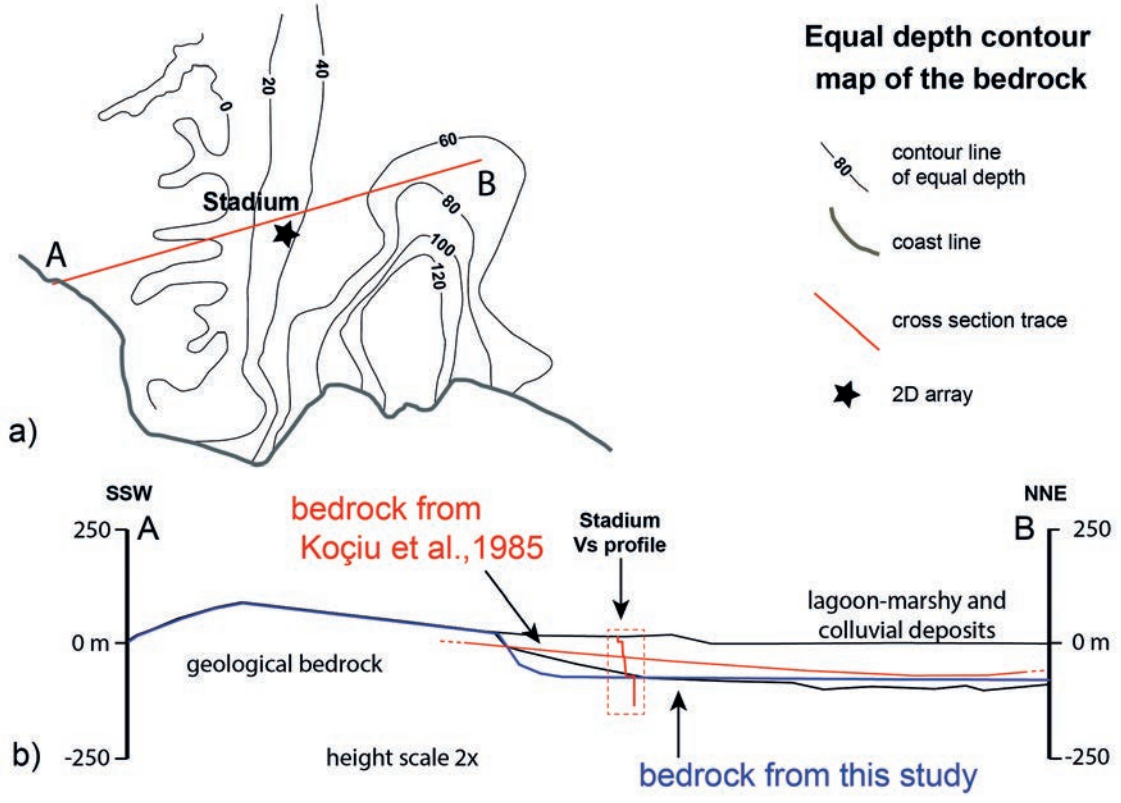

Fig. 17 - Comparison of the top of the bedrock depth from the present study and that by Koçiu *et al*. (1985): a) contour map of the bedrock depth by Koçiu *et al*. (1985), redrawn and simplified (see also Fig. 6b), with trace of the cross-section of Fig. 4, in red; b) top of the bedrock depths from Koçiu *et al*. (1985), in red, and from the present study, in blue, and V_S profile from the stadium array plotted on the cross-section.

To carry out a quantitative analysis of the error between the methodology applied in this study and in the previous available study, we compare in Fig. 17 the bedrock depth deducible from Koçiu *et al*. (1985) and the one retrieved from Fig. 16.

We have plotted on Fig. 17b the top of the bedrock depth as reconstructed from the present study (blue line) and the one from Koçiu *et al*. (1985) (red line) along the SW-NE trending cross-section of Fig. 4. Despite the general similar trend, the bedrock top line by Koçiu *et al*. (1985) gently dips to NE and has a more smoothed profile than the bedrock from our reconstruction. On the other hand, the bedrock from this study has a more stepped profile in the western part of the cross-section, but better fits with the geological data in the tract from the stadium to the north-eastern termination. It seems quite evident a good correspondence between the bedrock depth from ambient vibration data and the geological boundary between the lagoon-marshy and colluvial deposits and the underlying geological bedrock. Moreover, on the cross-section it has also been plotted the V_S profile from the stadium array, which shows an increment of V_S close to the depth of our reconstructed bedrock.

7. Conclusions

The results obtained in this study can be considered a preliminary step towards the seismic zoning of the city. They allow us defining three seismically homogeneous zones in the historical centre and one in the most damaged area after the 21 September 2019 earthquake. Expected damages in the historical city centre could be particularly enhanced if the following conditions exist: the occurrence of higher resonance frequencies (3-10 Hz) and a peculiar building typology mainly consisting of old, highly vulnerable, two- to four-storey masonry buildings.

Moreover, the results from array noise measurements at the stadium highlight the necessity of performing laboratory tests for thoroughly investigating the geotechnical properties of the soil in the eastern historical centre, where a thick cover of Quaternary marshy deposits is present and very poor soil mechanical properties are expected.

The map of the geological bedrock was obtained despite the fact that relatively large errors may affect the depth estimates provided by this approach (D'Amico *et al*., 2008). However, it can be considered as a useful proxy for more costly exploratory surveys: it provides useful information for the planning of the new field campaign and new data acquisitions, enhancing the importance of the use of joint inversion for investigating the city subsoil and fixing the maximum depth exploration.

Eventually, these preliminary results may give useful information on the post-earthquake reconstruction and the enhancement of urban resilience.

Supplementary material related to this article (E S1 - Table of the SESAME (2004) criteria applied to DU1-DU15 measurements and E S2 - Table of the SESAME (2004) criteria applied to DU16-DU29 measurements) is available online at the BGTA website www.bgta.eu.

Acknowledgements. The activities shown in this manuscript were carried out within the framework of the CNR/MOES Joint research project "Seismic risk assessment in cultural heritage cities of Albania" in the biennium 2018-2019 (https://www.cnr.it/en/bilateralagreements/agreement/60/moes-ministry-of education-and-sport-of-therepublic-of-albania). Two anonymous reviewers are acknowledged for their careful revision and for providing useful comments and suggestions that strongly improved the manuscript.

REFERENCES

Aki K.; 1957: *Space and time spectra of stationary stochastic waves, with special reference to microtremors*. Bull. Earthquake Res. Inst., **35**, 415-456.

Aki K.; 1965: *A note on the use of microseisms in determining the shallow structure of the Earth's crust*. Geophys., **30**, 665-666.

Aliaj Sh., Melo V., Hyseni A., Skrami J., Mehillka L., Muço B., Sulstarova E., Prifti K., Pashko P. and Prillo S.; 1996: *Struktura neotektonike e Shqiperise dhe evolucioni gjeodinamik i saj*. Archive of Institute of Seismology, Tirana, Albania, 497 pp.

Aliaj Sh., Koçiu S., Muço B. and Sulstarova E.; 2010: *Sizmiciteti, sizmotektonika dhe vleresimi i rrezikut sizmik në Shqipëri*. Akademia e Shkencave e Shqipërisë, Tirana, Albania, 310 pp.

Ashayeri I., Sadr A., Biglari M. and Haghshenas E.; 2020: *Comprehensive ambient noise analyses for seismic microzonation of Sarpol-e-zahab after the Mw 7.3 2017 Iran earthquake*. Eng. Geol., **272**, 105636, doi: 10.1016/j.enggeo.2020.105636.

Bettig B., Bard P.Y., Scherbaum F., Riepl J., Cotton F., Cornou C. and Hatzfeld D.; 2005: *Analysis of dense array noise measurements using the modified spatial auto-correlation method (SPAC): application to the Grenoble area*. Boll. Geof. Teor. Appl., **42**, 281-304.

Birgören G., Özel O. and Siyahi B.; 2009: *Bedrock depth mapping of the coast south of Istanbul: comparison of analytical and experimental analyses*. Turkish J. Earth Sci., **18**, 315-329.

BSSC; 2003: *NEHRP recommended provisions for seismic regulations for new buildings and other structures (FEMA-450)*. Building Seismic Safety Council, Federal Emergency Management Agency, Washington, DC, USA, 356 pp.

Caielli G., de Franco R., Di Fiore V., Albarello D., Catalano S., Pergalani F., Cavuoto G., Cercato M., Compagnoni M., Facciorusso J., Famiani D., Ferri F., Imposa S., Martini G., Paciello A., Paolucci E., Passeri F., Piscitelli S., Puzzilli L.M. and Vassallo M.; 2020: *Extensive surface geophysical prospecting for seismic microzonation*. Bull. Earthquake Eng., **18**, 5475-5502, doi: 10.1007/s10518-020-00866-4.

Castellaro S. and Mulargia F.; 2009: *The effect of velocity inversions on H/V*. Pure Appl. Geophys., **166**, 567-592.

CEN (Comité Européen de Normalisaton); 2004: *EN 1998-1. Eurocode 8: Design of structures for earthquake resistance - Part 1: General rules, seismic actions and rules for buildings*. European Committee for Standardization, Brussels, Belgium, 229 pp.

D'Amico V., Picozzi M., Baliva F. and Albarello D.; 2008: *Ambient noise measurements for preliminary site-effects characterization in the urban area of Florence, Italy*. Bull. Seismol. Soc. Am., **98**, 1373-1388, doi: 10.1785/0120070231.

Del Monaco F., Tallini M., De Rose C. and Durante F.; 2013: *HVNSR survey in historical downtown L'Aquila (central Italy): site resonance properties vs. subsoil model*. Eng. Geol., **158**, 34-47, doi: 10.1016/j.enggeo.2013.03.008.

Delgado J., López Casado C., Estévez A., Giner J., Cuenca A. and Molina S.; 2000a: *Mapping soft soils in the Segura River valley (SE Spain): a case study of microtremors as an exploration tool*. J. Appl. Geophys., **45**, 19-32.

Delgado J., López Casado C., Giner J., Estévez A., Cuenca A. and Molina S.; 2000b: *Microtremors as a geophysical exploration tool: applications and limitations*. Pure Appl. Geophys., **157**, 1445-1462.

Di Giacomo D., Gallipoli M.R., Mucciarelli M., Parolai S. and Richwalski S.M.; 2005: *Analysis and modeling of HVSR in the presence of a velocity inversion: the case of Venosa, Italy*. Bull. Seismol. Soc. Am., **95,** 2364-2372.

Duni L. and Theodoulidis N.; 2020: *Short note on the 26 November 2019, Durres (Albania) M 6.4 earthquake: strong ground motion with emphasis in Durres city*. 15 pp., <www.emsc-csem.org/Files/news/Earthquakes_reports/Short-Note_EMSC_31122019.docx> (accessed on 10 January 2020).

Fairchild G.M., Lane J.W., Voytek E.B. and LeBlanc D.R.; 2013: *Bedrock topography of western Cape Cod, Massachusetts, based on bedrock altitudes from geologic borings and analysis of ambient seismic noise by the horizontal-to-vertical spectral-ratio method*. U.S.G.S., Scientific Investigations Map 3233, Northborough, MA, USA, 17 pp. <pubs.usgs.gov/sim/3233> (accessed 20 Feb 2017).

Foti S., Parolai S., Albarello D. and Picozzi M.; 2011: *Application of surface-wave methods for seismic site characterization*. Surv. Geophys., **32**, 777-825.

Gallipoli M.R., Calamita G., Tragni N., Pisapia D., Lupo M., Mucciarelli M., Stabile T.A., Perrone A., Amato L., Izzi F., La Scaleia G., Maio D. and Salvia V.; 2020: *Evaluation of soil-building resonance effect in the urban area of the city of Matera (Italy)*. Eng. Geol., **272**, 105645, doi: 10.1016/j.enggeo.2020.105645.

Gaudiosi I., Del Monaco F., Milana G. and Tallini M.; 2014: *Site effects in the Aterno River Valley (L'Aquila, Italy): comparison between empirical and 2D numerical modelling starting from April 6th 2009 Mw 6.3 earthquake*. Bull. Earthquake Eng., **12**, 697-716, doi: 10.1007/s10518-013-9540-6.

Giallini S., Pizzi A., Pagliaroli A., Moscatelli M., Vignaroli G., Sirianni P., Mancini M. and Laurenzano G.; 2020: *Evaluation of complex site effects through experimental methods and numerical modelling: the case history of Arquata del Tronto, central Italy*. Eng. Geol., **272**, 105646, doi: 10.1016/j.enggeo.2020.105646.

Gosar A., Rošer J., Šket Motnikar B. and Zupančič P.; 2010: *Microtremor study of site effects and soil-structure resonance in the city of Ljubljana (central Slovenia)*. Bull. Earthquake Eng., **8**, 571-592, doi: 10.1007/s10518-009-9113-x.

Gruppo di Lavoro MS; 2008: *Indirizzi e criteri per la microzonazione sismica*. Conferenza delle Regioni e delle Province Autonome, Dipartimento della Protezione Civile, Roma, Italy, 3 vol. and Dvd.

Harutoonian P., Leo C.J., Tokeshi K., Doahn T., Castellaro S., Zou J.J., Liyanapathirana D.S. and Wong H.; 2013: *Investigation of dynamically compacted ground by HVSR-based approach*. Soil Dyn. Earthquake Eng., **46**, 20-29, doi: 10.1016/j.soildyn.2012.12.004.

Hinzen K.-G., Scherbaum F. and Weber B.; 2004: *On the resolution of H/V measurements to determine sediment thickness, a case study across a normal fault in the Lower Rhine embayment, Germany*. J. Earthquake Eng., **8**, 909-926.

Ibs-von Seht M. and Wohlenberg J.; 1999: *Microtremor measurements used to map thickness of soft sediments*. Bull. Seismol. Soc. Am., **89**, 250-259.

ISSMGE; 1999: *Manual for zonation on seismic geotechnical hazards*. Technical Committee for Earthquake Geotechnical Engineering, TC4, International Society for Soil Mechanics and Geotechnical Engineering, 20 pp.

Koçiu S.; 2004: *Induced seismic impacts observed in coastal area of Albania: case studies*. In: Proc., 5th International Conference on Case Histories in Geotechnical Engineerig, New York, NY, USA, 9 pp.

Koçiu S., Sulstarova E., Aliaj Sh., Duni Ll., Peçi V., Konomi N., Dakoli H., Fuga I., Goga K., Zeqo A., Kapllani L., Kozmaj S. and Lika M.; 1985: *Mikrozonimi i qytetit te Durresit (Microzonation of Durres City)*. Archive of Seismological Institute, Tirana, Albania, Internal report.

Kodra A. and Naçi P.; 2012: *Harte Gjeologjike. Plansheti Durresi (Scale 1:25,000)*. Ministria e Ekonomisë, Tregtisë dhe Energjitikës, Sherbimi Gjeologjik Shqiptar, Tirana, Albania.

Konno K. and Ohmachi T.; 1998: *Ground-motion characteristics estimated from spectral ratio between horizontal and vertical components of microtremors*. Bull. Seismol. Soc. Am., **88**, 228-241.

Lacoss R., Kelly T.E.J. and Toksöz M.N.; 1969: *Estimation of seismic noise structure using arrays*. Geophys., **34**, 21-38, doi: 10.1190/1.1439995.

Laurenzano G., Barnaba C., Romano M.A., Priolo E., Bertoni M., Bragato P.L., Comelli P., Dreossi I. and Garbin M.; 2019: *The central Italy 2016-2017 seismic sequence: site response analysis based on seismological data in the Arquata del Tronto - Montegallo municipalities*. Bull. Earthquake Eng., **17**, 5449-5469, doi: 10.1007/s10518-018-0355-3.

Lekkas E., Mavroulis S., Filis Ch. and Carydis P.; 2019a: *The September 21, 2019 Mw 5.6 Durrës (Albania) earthquake*. Newsletter of Environmental, Disaster and Crises Management Strategies, **13**, 64, ISSN 2653-9454.

Lekkas E., Mavroulis S., Papa D. and Carydis P.; 2019b: *The November 26, 2019 Mw 6.4 Durrës (Albania) earthquake*. Newsletter of Environmental, Disaster and Crises Management Strategies, **15**, ISSN 2653-9454.

Lunedei E. and Malischewsky P.; 2015: *A review and some new issues on the theory of the H/V technique for ambient vibrations*. In: Ansal A. (ed), Perspectives on European Earthquake Engineering and Seismology, Springer, Berlin, Germany, Vol. 2, pp. 371-394, doi: 10.1007/978-3-319-16964-4_15.

Magnani M.; 1946: *Tettonica e sismicità nella regione Albanese*. Geofisica Pura e Applicata, **8**, 1-42.

Mavroulis S., Lekkas E., Carydis P. and Papa D.; 2020: *Factors controlling building damage distribution of the November 26 Mw 6.4 Albania earthquake*. In: Proc., EGU General Assembly 2020, Online, EGU2020-18616, doi: 10.5194/egusphere-egu2020-18616.

Meço S. and Aliaj S.; 2000: *Geology of Albania*. Beiträge zur Regionalen Geologie der Erde, Gebrüder Borntraeger, Berlin, Germany, Vol. 28, 246 pp.

Milana G., Azzara R.M., Bertrand E., Bordoni P., Cara F., Cogliano R., Cultrera G., Di Giulio G., Duval A.M., Fodarella A., Marcucci S., Pucillo S., Régnier J. and Riccio G.; 2011: *The contribution of seismic data in microzonation studies for downtown L'Aquila*. Bull. Earthquake Eng., **9**, 741-759, doi: 10.1007/s10518-011-9246-6.

Milana G., Cultrera G., Bordoni P., Bucci A., Cara F., Cogliano R., Di Giulio G., Di Naccio D., Famiani D., Fodarella A., Mercuri A., Pischiutta M., Pucillo S., Riccio G. and Vassallo M.; 2020: *Local site effects estimation at Amatrice (central Italy) through seismological methods*. Bull. Earthquake Eng., **18**, 5713-5739, doi: 10.1007/s10518-019-00587-3.

Moscatelli M., Albarello D., Scarascia Mugnozza G. and Dolce M.; 2020: *The Italian approach to seismic microzonation*. Bull. Earthquake Eng., **18**, 5425-5440, doi: 10.1007/s10518-020-00856-6.

Mucciarelli M. (a cura di); 2015: *Tecniche semplificate per la stima dell'amplificazione sismica e della dinamica degli edifici*. Aracne Editore, Ariccia, Italy, 448 pp., ISBN: 978-88-548-4495-7.

Mukhopadhyay S. and Bormann P.; 2004: *Low cost seismic microzonation using microtremor data: an example from Delhi, India*. J. Asian Earth Sci., **24**, 271-280, doi: 10.1016/j.jseaes.2003.11.005.

Naçi P., Kodra A. and Borova M.; 2012: *Harte Gjeologjike. Plansheti Vrinasi (Scale 1:25.000)*. Ministria e Ekonomisë, Tregtisë dhe Energjitikës, Sherbimi Gjeologjik Shqiptar, Tirana, Albania.

Nakamura Y.; 1989: *A method for dynamic characteristics estimation of subsurface using microtremor on the ground surface*. Railway Technical Research Institute, Quarterly Reports, **30**, 25-33.

Ohori M., Nobata A. and Wakamatsu K.; 2002: *A comparison of ESAC and FK methods of estimating phase velocity using arbitrarily shaped microtremor analysis*. Bull. Seismol. Soc. Am., **92**, 2323-2332.

Okada H.; 2003: *The microtremor survey method*. Society of Exploration Geophysicists, Tulsa, OK, USA, Geophysical Monograph Series, n. 12, 135 pp.

Ozalaybey S., Zor E., Ergintav S. and Tapirdamaz M.C.; 2011: *Investigation of 3-D basin structures in the Izmit Bay area (Turkey) by single-station microtremor and gravimetric methods*. Geophys. J. Int., **186**, 883-894, doi: 10.1111/j.1365-246X.2011.05085.x.

Park R., Miller D. and Xia J.; 1999: *Multichannel analysis of surface waves*. Geophys., **64**, 800-808.

Parolai S., Bormann P. and Milkereit C.; 2002: *New relationships between Vs, thickness of sediments, and resonance frequency calculated by the H/V ratio of seismic noise for the Cologne area (Germany)*. Bull. Seismol. Soc. Am., **92**, 2521-2527, doi: 10.1785/0120010248.

Pergalani F., Pagliaroli A., Bourdeau C., Compagnoni M., Lenti L., Lualdi M., Madiai C., Martino S., Razzano R., Varone C. and Verrubbi V.; 2020: *Seismic microzoning map: approaches, results and applications after the 2016-2017 central Italy seismic sequence*. Bull. Earthquake Eng., **18**, 5595-5629, doi: 10.1007/s10518-019-00640-1.

Sánchez-Sesma F.J.; 2017: *Modeling and inversion of the microtremor H/V spectral ratio: physical basis behind the diffuse field approach*. Earth Planets Space, **69**, 92, doi: 10.1186/s40623-017-0667-6.

Sandron D., Maskey S., Giorgi M., Maharjan D.K., Shrestha S.N., Cravos C. and Pettenati F.; 2019: *Environmental noise measurements in Lalitpur area (Kathmandu) after the M 7.8 Gorkha 2015 earthquake*. Boll. Geof. Teor. Appl., **60**, 17-38, doi: 10.4430/bgta0259.

SESAME; 2004: *Guidelines for the implementation of the H/V spectral ratio technique on ambient vibrations: measurements, processing and interpretation*. SESAME European Research project WP12 - Deliverable D23.12, European Commission - Research General Directorate, Brussels, Belgium, <ftp.geo.uib.no/pub/seismo/SOFTWARE/SESAME/USER-GUIDELINES/SESAME-HV-User-Guidelines.pdf>.

SESAME; 2005: *Recommendations for quality array measurements and processing*. SESAME European Research project WP13 - Deliverable D24.13, European Commission - Research General Directorate, Brussels, Belgium, <ftp.geo.uib.no/pub/seismo/ SOFTWARE/SESAME/USER-GUIDELINES/SESAME-HV-User-Guidelines.pdf>.

Thabet M.; 2019: *Site-specific relationships between bedrock depth and HVSR fundamental resonance frequency using KiK-NET data from Japan, June 2019*. Pure Appl. Geophys., **176**, 4809-4831, doi: 10.1007/s00024-019-02256-7.

Tün M., Pekkan E., Özel O. and Guney Y.; 2016: *An investigation into the bedrock depth in the Eskisehir Quaternary Basin (Turkey) using the microtremor method*. Geophys. J. Int., **207**, 589-607, doi: 10.1093/gji/ggw294.

UNDP; 2003: *Disaster risk assessment in Albania - Executive summary report*. United Nations Development Programme, Department for International Development, Disaster Management and Emergency Preparedness Project, Tirana, Albania, 105 pp.

Weatherill G.A., Pagani M. and Garcia J.; 2016: *Exploring earthquake databases for the creation of magnitude-homogeneous catalogues: tools for application on a regional and global scale*. Geophys. J. Int., **206**, 1652-1676, doi: 10.1093/gji/ggw232.

Corresponding author: Marco Mancini
Consiglio Nazionale delle Ricerche
Istituto di Geologia Ambientale e Geoingegneria (IGAG),
Area della Ricerca Roma 1
Via Salaria km 29,300, 00015 Monterotondo Scalo (Rome), Italy
Phone: +39 06 90672740; e-mail: marco.mancini@igag.cnr.it